Report

Cell Reports

SynDIG4/Prrt1 Is Required for Excitatory Synapse Development and Plasticity Underlying Cognitive Function

Graphical Abstract

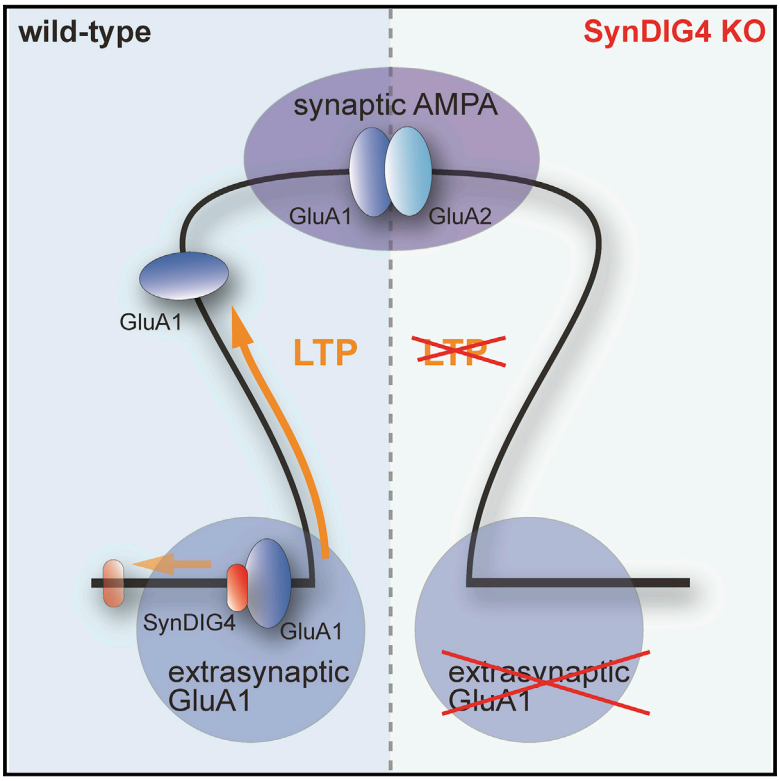

Highlights

- SynDIG4 affects AMPAR biophysical properties in a subunit-dependent manner
- Loss of SynDIG4 results in reduced extrasynaptic AMPAR and weaker synapses
- SynDIG4 is necessary for tetanus-induced, but not theta-burst, LTP
- SynDIG4 KO mice exhibit deficits in two independent cognitive behavior tasks

Authors

Lucas Matt, Lyndsey M. Kirk, George Chenaux, ..., Jacqueline N. Crawley, Johannes W. Hell, Elva Díaz

Correspondence

jwhell@ucdavis.edu (J.W.H.), ediaz@ucdavis.edu (E.D.)

In Brief

Matt et al. show that mice lacking the AMPAR-associated protein SynDIG4/Prrt1 display deficits in synaptic plasticity and cognition. SynDIG4 modifies AMPAR biophysical properties in heterologous cells, but synaptic AMPAR kinetics are unchanged, suggesting that SynDIG4 establishes a pool of extrasynaptic AMPARs necessary for higher-order cognitive plasticity.

Matt et al., 2018, Cell Reports *22*, 2246–2253
February 27, 2018
https://doi.org/10.1016/j.celrep.2018.02.026

CellPress

OPEN ACCESS
CellPress

Cell Reports
Report

SynDIG4/Prrt1 Is Required for Excitatory Synapse Development and Plasticity Underlying Cognitive Function

Lucas Matt,[1,4,5] Lyndsey M. Kirk,[1,4] George Chenaux,[1,4] David J. Speca,[1] Kyle R. Puhger,[2] Michael C. Pride,[2] Mohammad Qneibi,[3] Tomer Haham,[3] Kristopher E. Plambeck,[1] Yael Stern-Bach,[3] Jill L. Silverman,[2] Jacqueline N. Crawley,[2] Johannes W. Hell,[1,*] and Elva Díaz[1,6,*]

[1]Department of Pharmacology, UC Davis School of Medicine, Davis, CA 95616, USA
[2]MIND Institute, Department of Psychiatry and Behavioral Sciences, UC Davis School of Medicine, Sacramento, CA 95817, USA
[3]Department of Biochemistry and Molecular Biology, Institute for Medical Research Israel-Canada, The Hebrew University-Hadassah Medical School, Jerusalem 91120, Israel
[4]These authors contributed equally
[5]Present address: Department of Pharmacology, Toxicology and Clinical Pharmacy, Institute of Pharmacy, University of Tübingen, Tübingen 72074, Germany
[6]Lead Contact
*Correspondence: jwhell@ucdavis.edu (J.W.H.), ediaz@ucdavis.edu (E.D.)
https://doi.org/10.1016/j.celrep.2018.02.026

SUMMARY

Altering AMPA receptor (AMPAR) content at synapses is a key mechanism underlying the regulation of synaptic strength during learning and memory. Previous work demonstrated that *SynDIG1* (synapse differentiation-induced gene 1) encodes a transmembrane AMPAR-associated protein that regulates excitatory synapse strength and number. Here we show that the related protein SynDIG4 (also known as Prrt1) modifies AMPAR gating properties in a subunit-dependent manner. Young SynDIG4 knockout (KO) mice have weaker excitatory synapses, as evaluated by immunocytochemistry and electrophysiology. Adult SynDIG4 KO mice show complete loss of tetanus-induced long-term potentiation (LTP), while mEPSC amplitude is reduced by only 25%. Furthermore, SynDIG4 KO mice exhibit deficits in two independent cognitive assays. Given that SynDIG4 colocalizes with the AMPAR subunit GluA1 at non-synaptic sites, we propose that SynDIG4 maintains a pool of extrasynaptic AMPARs necessary for synapse development and function underlying higher-order cognitive plasticity.

INTRODUCTION

AMPA receptors (AMPARs) are responsible for fast excitatory synaptic transmission in the brain. AMPARs are implicated in plasticity mechanisms such as long-term potentiation (LTP) (Huganir and Nicoll, 2013) and synaptic scaling (Lee et al., 2014; Turrigiano, 2012). A diverse family of AMPAR auxiliary factors regulates AMPAR trafficking and gating (Jackson and Nicoll, 2011). Stargazin, the prototypical transmembrane AMPAR regulating protein (TARP), promotes surface expression and alters biophysical properties of AMPARs in heterologous cells such that they more closely resemble those of endogenous receptors (Chen et al., 2000). In addition to TARPs, several other unrelated protein families have been identified as auxiliary AMPAR factors with distinct and overlapping functions (Chen et al., 2000; Chen et al., 2014; Díaz, 2010; Jackson and Nicoll, 2011; Schwenk et al., 2009, 2014; Shanks et al., 2012; von Engelhardt et al., 2010).

SynDIG1 (synapse differentiation-induced gene 1) encodes a type II transmembrane protein that interacts with AMPARs in brain and heterologous cells and regulates synaptic strength (Kalashnikova et al., 2010). *SynDIG1* mutant mice exhibit deficits in excitatory synapse maturation (Chenaux et al., 2016). In contrast to other AMPAR accessory proteins, SynDIG1 does not regulate AMPAR dynamics (Lovero et al., 2013), suggesting that SynDIG1 is an atypical AMPAR auxiliary factor.

SynDIG defines a family of genes that encodes brain-specific transmembrane proteins (Kalashnikova et al., 2010). SynDIG4, also known as Prrt1 (proline-rich transmembrane protein 1), was identified in several independent proteomic studies as a candidate AMPAR-associated protein (Chen et al., 2014; Schwenk et al., 2012, 2014; Shanks et al., 2012; von Engelhardt et al., 2010), as well as a component of the postsynaptic density (PSD) (Jordan et al., 2004). Surprisingly, SynDIG4 is not enriched at synapses; the major fraction of SynDIG4 colocalizes with the AMPAR subunit GluA1 at extrasynaptic sites in rat cortical neurons (Kirk et al., 2016). Here we show that SynDIG4 plays a critical role in excitatory synapse function with a combination of electrophysiology, immunocytochemistry, biochemistry, and behavior. We propose that SynDIG4 maintains a pool of extrasynaptic AMPARs necessary for synapse development and function underlying higher-order cognitive plasticity.

RESULTS

SynDIG4 Modifies AMPAR Gating Kinetics in a Subunit-Dependent Manner

To test direct effects of SynDIG4 on AMPAR properties, heterologous expression in *Xenopus* oocytes and outside-out patch-clamp electrophysiological recordings were used to compare it

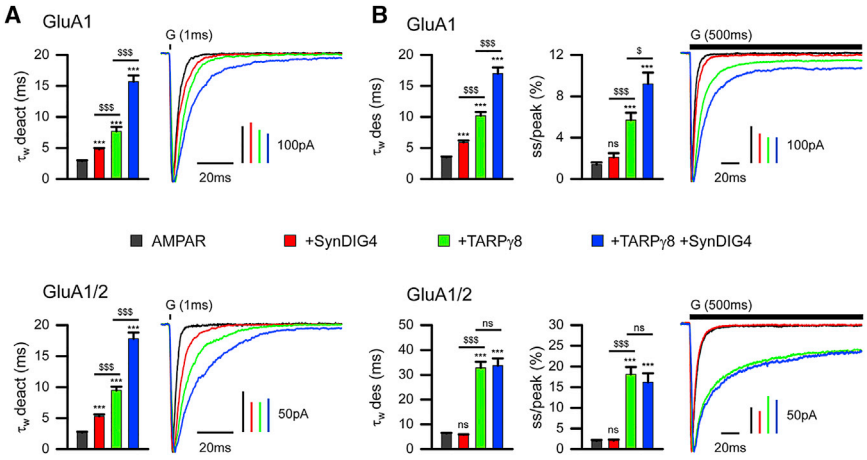

Figure 1. SynDIG4 Modifies AMPAR Gating Kinetics in a Subunit-Dependent Manner

(A and B) Representative normalized current responses of AMPAR recorded upon 1 ms (A) and 500 ms (B) application of 10 mM glutamate (G, indicated above the current trace) to giant outside-out patches excised from *Xenopus laevis* oocytes expressing homomeric GluA1 (top) and heteromeric GluA1/2 (bottom) alone (black) or in combination with SynDIG4 (red), TARPγ8 (green), or both (blue). Graphs summarize weighted time constants for deactivation (τ_W deact) and desensitization (τ_W des), as well as steady-state to peak current (ss/peak). Data shown are mean ± SEM; n = 10–20 patches.

Significance (one-way ANOVA): */$ $p < 0.05$; **/$$ $p < 0.01$; ***/$$$ $p < 0.001$; ns, not significant. See also Table S1.

with TARPγ8, which is highly expressed in hippocampus (Tomita et al., 2003). SynDIG4 slows deactivation kinetics of both GluA1 homomers and GluA1/2 heteromers, albeit less than TARPγ8; however, a synergistic effect was observed with both SynDIG4 and TARPγ8 (Figure 1A). SynDIG4 reduces desensitization of GluA1 homomers with or without TARPγ8 but has no significant effect on desensitization of heteromeric GluA1/2 (Figure 1B). SynDIG4 does not alter recovery from desensitization of GluA1 homomers or GluA1/2 heteromers (Table S1).

Expression Profile of Prrt1/SynDIG4 Mutant Reporter Mice

These results motivated investigation of a *SynDIG4* null reporter line [*Prrt1*$^{tm1(KOMP)Vlcg}$] obtained from the Knock Out Mouse Project (KOMP) consortium (Valenzuela et al., 2001), in which the SynDIG4 protein-coding region is replaced with a β-galactosidase (β-gal) cassette (Figure 2A). The resulting reporter protein, driven by the SynDIG4 promoter, is retained within the soma. To verify loss of SynDIG4 protein, brain lysates were collected from homozygous mutant mouse (referred to here as *SynDIG4*$^{-/-}$) and compared with wild-type (WT) littermates at postnatal day (P) 14. No detectable levels of SynDIG4 in postnuclear (S1), membrane (P2), synaptosomal (Syn), or PSD-enriched fractions were detected in *SynDIG4*$^{-/-}$ mice (Figure 2B). PSD-95 was enriched and synaptophysin was undetectable in PSD fractions, while β-actin indicated equivalent loading between fractions.

To investigate potential changes in subcellular composition of mutant brain tissue, candidate synaptic proteins were analyzed (Table S2). Except for an increase in GluA2 in the synaptosomal fraction of *SynDIG4*$^{-/-}$ samples ($p = 0.045$), there were no significant changes in glutamate receptor subunits (GluA1, GluA2, GluN1, and GluN2B), and the distribution of synaptic scaffolds PSD-93 or PSD-95 was not altered in *SynDIG4*$^{-/-}$ (Figures S1A–S1D).

To investigate SynDIG4 expression *in vivo*, mutant mouse brain sections were stained for β-gal activity. Sagittal sections from P7 *SynDIG4*$^{-/-}$ mice show β-gal reporter activity throughout hippocampus, with weak expression in olfactory bulb and neocortex (Figure S1E). Coronal sections of P14, P28, and P62 brains show β-gal expression remains high throughout hippocampus and increased in olfactory bulb and neocortex (Figure S1F).

Reduced Extrasynaptic AMPARs and Weaker Synapses in *SynDIG4*$^{-/-}$ Mice

To investigate effects of SynDIG4 deficiency, a combination of electrophysiology and immunocytochemistry was employed. Dissociated hippocampal neurons from WT and *SynDIG4*$^{-/-}$ littermates were fixed and stained for GluA1 at synapses (defined as overlap with vGlut1) and at extrasynaptic sites (defined as no overlap with vGlut1) at 14 days *in vitro* (DIV) (Figure 2C). We observed decreased GluA1 density at extrasynaptic sites and a corresponding increased density of GluA1 at synapses in *SynDIG4*$^{-/-}$ neurons compared with WT (Figure 2D; Table S1). GluA1 puncta size and intensity were reduced at both synaptic and extrasynaptic sites in *SynDIG4*$^{-/-}$ neurons compared with WT (Figures 2E and 2F; Table S1). We did not observe significant changes in synaptic GluA2 puncta; however, extrasynaptic GluA2 puncta density was significantly reduced (Figures S2A and S2B).

Extrasynaptic AMPARs are localized to different locations: mobile pools at the cell surface and intracellular compartments, including recycling endosomes and transport vesicles that might not be fully captured in our analysis of extrasynaptic puncta. Therefore, we evaluated the level and area of total GluA1 and GluA2 signal that does not overlap with vGlut1; similar results were obtained with this analysis (Table S3). *SynDIG4*$^{-/-}$ neurons did not show significant differences in dendrite complexity compared with WT (Figures S2C and S2D). Staining with primary antibodies individually and both secondary antibodies indicated no cross-reactivity or bleed-through that might contribute to the immunofluorescence signal observed (Figures S2E and S2F).

To assess whether the change in AMPAR distribution reflected functional alterations, acute slices from 2- to 3-week-old WT and *SynDIG4*$^{-/-}$ mice were used in whole-cell patch-clamp experiments. Miniature excitatory postsynaptic currents (mEPSCs) were recorded in hippocampal CA1 pyramidal cells (Figures 2G and 2H). The mEPSC amplitude in *SynDIG4*$^{-/-}$

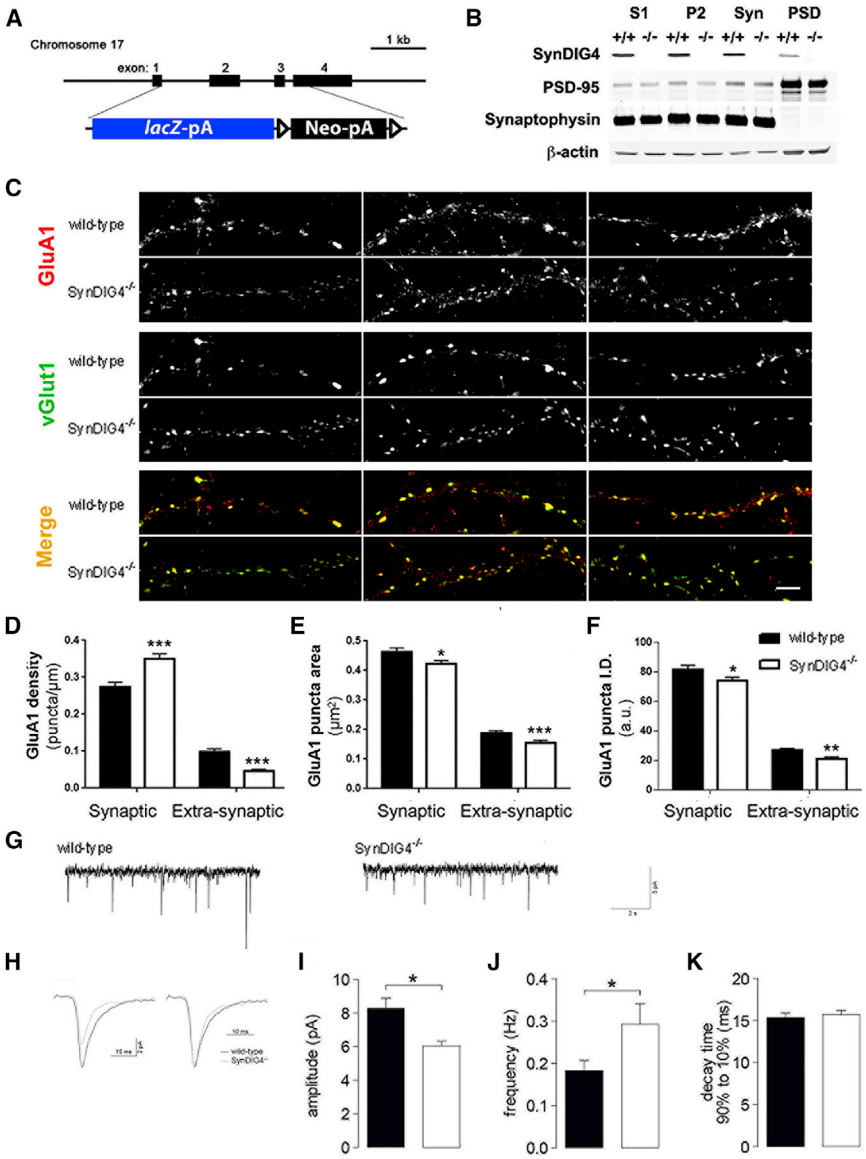

Figure 2. Loss of SynDIG4 Leads to Altered GluA1 Distribution and Weaker Synapses

(A) Schematic showing the replacement of the coding region of the *SynDIG4* locus with a *lacZ* reporter and *loxP*-flanked neomycin selection cassette.

(B) Immunoblots (10 μg of protein loaded per lane) stained for SynDIG4, PSD-95, synaptophysin, and β-actin show postnuclear (S1), membrane (P2), synaptosomal (Syn), and PSD biochemical fractions from postnatal day (P14) WT (+/+) and *SynDIG4* homozygous mutant (−/−) mouse brain tissue.

(C–F) Primary dissociated hippocampal cultures (14 DIV) were used for immunocytochemistry. Representative images of WT and *SynDIG4*$^{-/-}$ neurons stained with GluA1 and vGlut1 (C). Graphs depict quantification of synaptic (colocalized with vGlut1) and extrasynaptic (no colocalization with vGlut1) GluA1 puncta density (D), area (E), and integrated density (ID) (F). Data are averaged from two independent experiments; n = 24–25 cells per genotype per experiment, and three dendrites per cell were selected for measurement. Scale bar, 5 μm.

(G–K) Hippocampal pyramidal neurons in acute slices from 12- to 15-day-old mice were used to record AMPAR mEPSC at −70 mV. Traces from representative recordings (G). Averaged events from one representative cell per genotype are presented to scale (left) and normalized to peak (right) (H). Graphs represent average mEPSC amplitude (I), frequency (J), and decay time (K) in *SynDIG4*$^{-/-}$ and WT mice.

Significance (Student's t test): *p < 0.05, ***p < 0.001. See also Figures S1 and S2 and Tables S1, S2, and S3.

acute slices was significantly reduced and the mEPSC frequency was increased compared to WT (Figures 2I and 2J; Table S1). However, there was no significant difference in decay kinetics between WT and *SynDIG4*$^{-/-}$ neurons (Figure 2K; Table S1).

SynDIG4$^{-/-}$ Mice Show Impaired Schaffer-Collateral LTP

To test synaptic transmission, we recorded excitatory postsynaptic potentials (EPSPs) as extracellular field potentials (fEPSPs) in 8- to 12-week-old mice. By applying paired pulses, we did not observe alterations in presynaptic facilitation in *SynDIG4*$^{-/-}$ mice (Figure S3A). No differences were detected in signal strength in relation to stimulus intensity (Figure S3B). To test synaptic plasticity, we induced LTP of Schaffer-collateral synapses using a single 100 Hz/1 s tetanus, a paradigm that successfully elicits significant LTP in WT mice. Surprisingly, *SynDIG4*$^{-/-}$ synapses were not potentiated following tetanic stimulation; rather, there was a slight depression in transmission strength (Figure 3A; Table S1). To test whether LTP induction in *SynDIG4*$^{-/-}$ mice was generally impaired, we recorded LTP induced with 10 theta-burst stimulations, a different stimulus paradigm also known to elicit robust LTP in Schaffer-collateral synapses. TBS produced robust LTP in 8- to 12-week-old WT mice, as well as *SynDIG4*$^{-/-}$ mice (Figure 3B; Table S1). These results were recapitulated in 2- to 4-week-old animals (Figures S3C and S3D).

To investigate further the difference in LTP between WT and *SynDIG4*$^{-/-}$, we used the pairing-induced LTP paradigm in which the presynaptic high-frequency stimulus is applied while the postsynaptic cell is depolarized using a patch electrode. Pairing removes the Mg^{2+} block from the NMDA-type receptor (NMDAR), forgoing the necessity of AMPAR-dependent postsynaptic depolarization. We found no difference in pairing-induced LTP between 2-week-old WT and *SynDIG4*$^{-/-}$ neurons (Figure 3C; Table S1).

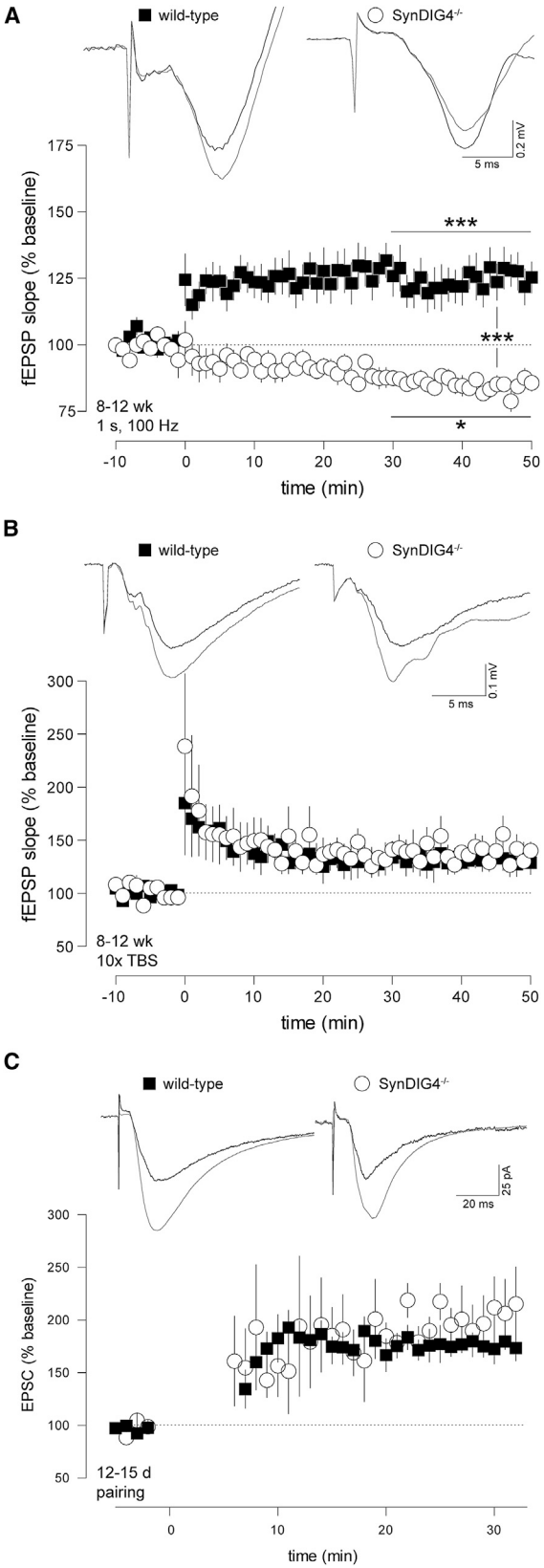

Figure 3. LTP Induction by a Single Tetanus, but Not by Theta-Burst or Pairing Stimulation, Is Impaired in *SynDIG4*$^{-/-}$ Mice

(A and B) Schaffer-collateral fEPSPs were recorded from acute forebrain slices of 8- to 12-week-old mice. A 100 Hz/1 s tetanus elicited LTP in WT mice while leading to a depression of the fEPSP slope in *SynDIG4*$^{-/-}$ mice (A). Theta-burst stimulus (TBS) led to robust LTP in *SynDIG4*$^{-/-}$ mice that was not significantly different from LTP in WT (B).

(C) Hippocampal pyramidal neurons in acute slices from 12- to 15-day-old mice were used to record evoked EPSC in whole-cell patch-clamp configuration following Schaffer-collateral stimulation. Cells were held at −70 mV to record AMPAR-mediated currents. LTP elicited by pairing presynaptic stimulation with postsynaptic depolarization to 0 mV was not significantly different in cells from *SynDIG4*$^{-/-}$ mice compared to WT.

Insets show sample traces before (black) and 30 min after (gray) tetanization. Significance is calculated by one-way ANOVA with Bonferroni's post-test between baseline and tetanized for each genotype and between tetanized of both genotypes. See also Figure S3 and Table S1.

SynDIG4 KO Mice Display Deficits on Two Independent Cognitive Tasks

We investigated the impact of SynDIG4 deletion on cognitive function *in vivo* using two established learning and memory tasks: Morris water maze and novel object recognition. A battery of general health parameters did not indicate any significant differences that might contribute to behavioral analysis (Table S4).

In the Morris water maze assay, mice were trained over a period of 5 days to swim to a hidden, submerged platform using visual cues, according to methods previously described (Brielmaier et al., 2012). The average latency to find the platform decreased over the training period for WT animals, while the average latency for *SynDIG4*$^{-/-}$ mice only decreased slightly and was significantly different when compared to WT animals (Figure 4A; Table S1). After the last training trial, the platform was removed and mice underwent a probe trial to measure time spent exploring the target quadrant that previously contained the hidden platform. WT mice spent significantly more time in the target quadrant than in the other three quadrants, in contrast to *SynDIG4*$^{-/-}$ mice (Figure 4B; Table S1), confirming that the deficit in spatial learning was caused by failure to use distal environmental cues to acquire the spatial location of the hidden platform.

We further tested whether *SynDIG4*$^{-/-}$ mice had deficits in a second cognitive task with different sensory and motor demands: the novel object recognition task (Brielmaier et al., 2012; Cohen et al., 2013; Vogel-Ciernia and Wood, 2014). Given a choice between two neutral objects of equal salience but with differing shapes and textures, one familiar and one novel, rodents will usually spend more time investigating the novel object. As previously described (Yang et al., 2015), mice were first habituated to the open-field testing environment, and a familiarization session with two identical objects indicated no left-right biases in either genotype (Figure 4C; Table S4). After exposure to the two identical objects, the chamber was cleaned and animals were allowed to explore one of the now-familiar objects and one novel object. WT mice displayed normal novel object recognition, spending significantly more time investigating the novel object than the familiar object. *SynDIG4*$^{-/-}$ mice failed to display novel object recognition, spending approximately equal time with the novel and the familiar objects (Figure 4D; Table S4).

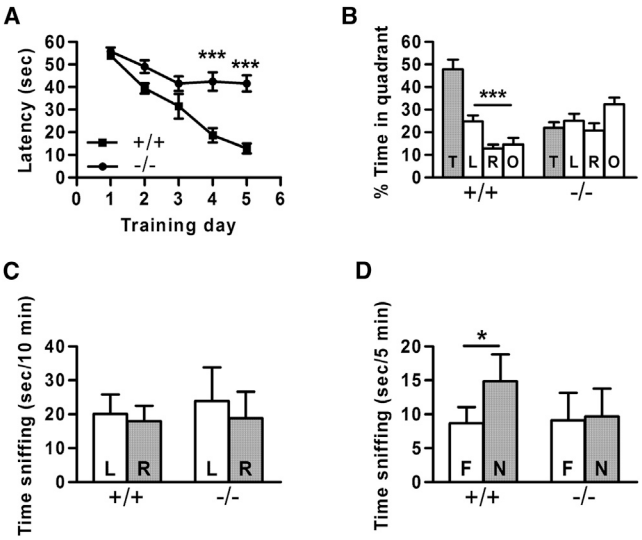

Figure 4. *SynDIG4*$^{-/-}$ Mice Are Deficient in Two Cognitive Learning and Memory Tasks

(A) Latency to find a hidden platform did not decrease significantly in *SynDIG4*$^{-/-}$ mice over a 5-day training period. Asterisks indicate significant differences in latency between WT (+/+) and *SynDIG4* homozygous mutant (−/−) mice on days 4 and 5.

(B) During the probe trial, WT mice spent significantly more time in the target quadrant than in other quadrants, whereas *SynDIG4*$^{-/-}$ mice did not. Quadrants: T, target; L, left; R, right; O, opposite.

(C) Neither WT nor *SynDIG4*$^{-/-}$ mice exhibited left-right bias in the habituation session of the novel object recognition task. L, left object; R, right object.

(D) WT mice spent significantly more time investigating the novel object (N) than the familiar object (F), while *SynDIG4*$^{-/-}$ animals showed no preference, indicating a deficit in object recognition.

For all experiments, WT, n = 9; *SynDIG4*$^{-/-}$, n = 11. Significance: *p < 0.05, ***p < 0.001.

See also Figure S4 and Tables S1 and S4.

We observed moderately higher exploratory activity in *SynDIG4*$^{-/-}$ mice compared to WT in the open field (Figures S4A and S4B). On the elevated plus-maze, more open arm time and entries were seen in *SynDIG4*$^{-/-}$ mice compared to WT; however, total number of entries was elevated (Figures S4C and S4D), indicating higher general exploratory activity rather than reduced anxiety-related behavior. Similarly, the number of light ↔ dark transitions was higher in *SynDIG4*$^{-/-}$ mice than in WT (Figures S4E and S4F). Higher exploratory locomotion in *SynDIG4*$^{-/-}$ mice in these three assays suggests that deficits in cognitive function are unlikely to be due to a motor disability.

DISCUSSION

Although SynDIG4 shares sequence similarity with SynDIG1, it has distinct expression in rat brain and is enriched with GluA1-containing AMPARs at extrasynaptic sites (Kirk et al., 2016). Based on the results presented here, we propose that SynDIG4 establishes a pool of extrasynaptic AMPARs necessary for synapse development and function underlying higher-order cognitive plasticity.

SynDIGs belong to a larger superfamily, named dispanin, based on sequence similarity (Sällman Almén et al., 2012). However, SynDIG4/Prrt1 shares only 35% sequence similarity with SynDIG1. In contrast to other AMPAR-associated transmembrane proteins, SynDIG1 does not promote AMPAR surface expression or alter channel gating when coexpressed with GluA1/2 subunits in HEK cells (Lovero et al., 2013), suggesting that SynDIG1 is an atypical AMPAR auxiliary factor. We tested whether coexpression of SynDIG1 altered biophysical properties of AMPARs in oocytes, and we did not find significant changes (data not shown), consistent with results in HEK cells (Lovero et al., 2013). However, there was a significant and high reduction in total current amplitude measured by whole-cell two-electrode voltage-clamp (TEVC) recordings (data not shown), so there may be minor changes associated with SynDIG1 coexpression that we could not detect in oocytes.

In contrast, SynDIG4 influences AMPAR gating properties in a subunit-dependent manner. We did not measure whether SynDIG4 influences AMPAR surface expression in oocytes directly. However, average current amplitude measured by TEVC recordings in the presence of the desensitization blocker cyclothiazide indicated ~35% reduction for GluA1 coexpressed with SynDIG4 ($p = 0.02$) and ~20% reduction for GluA1/2 coexpressed with SynDIG4 that did not reach significance ($p = 0.06$). These results are consistent with the outside-out patch recordings for SynDIG4. There was no correlation between current amplitude and the decay time in patch-clamp current recordings. That is, comparing currents with the same amplitude with or without SynDIG4 (as well as with or without TARPγ8) exhibited a significant slower deactivation in the presence SynDIG4. Therefore, we have not explored this observation further, although SynDIG4 might negatively affect surface delivery of AMPARs. These data support a direct and specific interaction of SynDIG4 with GluA1-containing AMPARs. SynDIG4 increased deactivation of GluA1 or GluA1/2 in oocytes, yet no significant change in decay time of mEPSC events in *SynDIG4*$^{-/-}$ neurons was observed, suggesting that SynDIG4 does not modulate GluA1 at synapses. In addition, we observed synergistic effects on AMPAR biophysical properties upon coexpression of both SynDIG4 and TARPγ8, indicating that these accessory proteins can interact simultaneously with AMPARs. TARPγ8 is a critical Ca^{2+}/calmodulin-dependent protein kinase IIa (CaMKIIa) substrate for hippocampal LTP, learning, and memory (Park et al., 2016). Future studies are needed to address the relationship, if any, between SynDIG4 and TARPγ8-dependent LTP.

Although SynDIG4 primarily colocalizes with GluA1-containing AMPARs at extrasynaptic sites, biochemical fractionation indicates a portion of SynDIG4 is present in the PSD-enriched fraction (Kirk et al., 2016). One possibility is that SynDIG4 traffics with GluA1-containing AMPARs between extrasynaptic and synaptic sites, perhaps due to an activity-dependent post-translational modification. For example, a CCFW motif in the juxta-transmembrane-associated region is conserved in all SynDIG proteins. The two cysteine residues in SynDIG1 are palmitoylated in an activity-dependent manner to regulate stability, localization, and function (Kaur et al., 2016) and preliminary experiments indicate that SynDIG4 is also palmitoylated (data not shown). It will be informative to investigate the relationship, if any, between

SynDIG4 palmitoylation and its role in synapse function. However, the SynDIG family does not contain a recognizable intracellular domain such as a PDZ binding motif, and it is unclear how SynDIG proteins are localized at synapses. Therefore, an alternative model is that SynDIG4 might physically restrain GluA1-containing AMPARs at extrasynaptic sites to maintain an extrasynaptic pool of AMPARs. Upon stimulation, SynDIG4 might release GluA1-containing AMPARs from extrasynaptic sites and allow other auxiliary factors such as TARPγ8 to transport them to synapses. Given that SynDIG4 increased deactivation of GluA1 and GluA1/2 in oocytes yet no significant change in decay time of mEPSC events in *SynDIG4*$^{-/-}$ neurons was observed, we interpret these results as evidence that SynDIG4 does not act primarily on synaptic AMPARs. However, SynDIG4 is not the only protein in which heterologous cell expression did not match the phenotype observed *in vivo*. For example, CKAMP44, which is a synaptic protein interacting with synaptic AMPARs, also slows AMPAR deactivation and is additive to TARPγ8; however, there was no effect on mEPSC decay time upon overexpression or in CKAMP44 knockout (KO) mice (von Engelhardt et al., 2010). The reason for the discrepancy is still not known. While we interpret our result as evidence for a primary role of SynDIG4 on extrasynaptic AMPARs, which is consistent with its localization, our findings do not rule out a direct role of SynDIG4 on synaptic AMPARs.

A particularly intriguing aspect of this study is that synaptic plasticity is disrupted in *SynDIG4*$^{-/-}$ mice when tetanic stimulation is used to induce plasticity, while TBS is normal. A previous study showed that TBS-induced LTP can be induced in GluA1 null mice, whereas tetanic-induced LTP cannot (Romberg et al., 2009). Given that SynDIG4 preferentially colocalizes with GluA1-containing AMPARs at non-synaptic sites (Kirk et al., 2016), and loss of SynDIG4 significantly reduces non-synaptic GluA1 and GluA2 shown here, these data are consistent with a model by which SynDIG4 selectively regulates an extrasynaptic pool of AMPARs during tetanic-induced LTP. Evidence suggests that LTP requires a reserve pool of extrasynaptic glutamate receptors independent of receptor subunit type (Granger et al., 2013). Furthermore, GluA1/2 heteromers constitute 95% of the extrasynaptic AMPAR pool (Lu et al., 2009), consistent with the observed reduced density of extrasynaptic GluA1/2 in *SynDIG4*$^{-/-}$ neurons. The importance of SynDIG4 in cognitive plasticity is underscored by the deficit in two independent mouse learning and memory behaviors.

The ~25% reduction in mEPSC amplitude in *SynDIG4*$^{-/-}$ neurons reflects a reduction in postsynaptic AMPAR responses, which could contribute to a decrease in tetanus-induced LTP by decreasing NMDAR channel activity, but it cannot explain the complete lack of LTP that we observe. More than 50% inhibition of AMPARs by 20 μM GYKI52466 or 0.25 μM NBQX does not diminish induction of LTP by tetanic stimulation in CA1 fEPSP recordings (Kapus et al., 2000). Furthermore, knockdown of PORCN, which fosters AMPAR secretory trafficking, reduces AMPAR mEPSC amplitude by ~25%, as does SynDIG4 KO. However, it only reduces LTP induced by 100 Hz/1 s stimulation proportional to the degree it reduces basal postsynaptic AMPAR responses, while the magnitude of LTP relative to basal synaptic transmission is the same in WT and PORCN knockdown neurons (Erlenhardt et al., 2016). Similarly, in knockin mice in which the last 4 residues of TARPγ8 were deleted to impair PSD-95 binding, postsynaptic AMPAR activity was reduced by ~40%, but the degree of tetanus-induce LTP relative to basal synaptic transmission was comparable between WT and knockin mice (Sumioka et al., 2011). Thus, it seems unlikely that a 25% reduction in postsynaptic AMPAR activity would by itself abolish tetanus-induced LTP in *SynDIG4*$^{-/-}$ mice. Abrogation of LTP induced by tetanic stimulation, but not by TBS or pairing, is consistent with the possibility that SynDIG4 is necessary for certain forms of synaptic plasticity through its role to establish an extrasynaptic pool of AMPARs that might also be needed to maintain normal basal synaptic function involving AMPAR trafficking.

The proline-rich N terminus of SynDIG4/Prrt1 is shared with Prrt2 (67% sequence similarity,) and Prrt2 has been identified as a candidate AMPAR-associated protein (Chen et al., 2014; Schwenk et al., 2012, 2014; Shanks et al., 2012; von Engelhardt et al., 2010). However, a study demonstrated a presynaptic role for Prrt2 in regulated exocytosis of neurotransmitter via interaction with synaptotagmin (Valente et al., 2016). Presynaptic release failure is a valid concern in the interpretation of tetanic stimulation-induced LTP for *SynDIG4*$^{-/-}$ mice discussed earlier. However, paired-pulse facilitation is not affected. We recognize that this result does not rule out all possible presynaptic deficiencies, but it does not indicate possible defects either. Furthermore, the input-output relationship is unaltered (if anything, *SynDIG4*$^{-/-}$ displays a tendency for increased fEPSP slope). If release probability was altered, we would expect differences either at high or at low stimulus intensities, depending on the deficit (Ca^{2+} sensitivity of the release machinery versus vesicle loading or density). Moreover, mEPSC frequency in *SynDIG4*$^{-/-}$ is increased. If release probability was decreased (to account for reduced LTP) we would expect a reduction in mEPSC frequency. The increase in mEPSC frequency could also reflect a postsynaptic effect by activating silent synapses in *SynDIG4*$^{-/-}$ to which extrasynaptic GluA1-containing AMPARs are recruited (indicated by increased synaptic GluA1 in *SynDIG4*$^{-/-}$). The reduction in mEPSC amplitude may reflect the reduction of synaptic GluA1 puncta area and intensity. Altogether, it is unlikely that presynaptic effects are the reason for the reduced LTP; however, we cannot rule out this possibility at present.

Given that both SynDIG1 and SynDIG4 are expressed in hippocampus, it is not unexpected that there are some similarities in phenotypes. For example, we observed that loss of SynDIG4 leads to increased synapse number similar to that observed in *SynDIG1* mutant mice (Chenaux et al., 2016). The increased synapse density observed in *SynDIG4*$^{-/-}$ or *SynDIG1* mutant mice could be a consequence of reduced synaptic strength. Homeostatic mechanisms lead to an increase in synapse number in the absence of potentiation to maintain total input strength (Bourne and Harris, 2011; Turrigiano, 2008). However, there are key differences between phenotypes in *SynDIG4*$^{-/-}$ and *SynDIG1* mutant mice that illustrate the unique role of SynDIG4 in synapse function. First, the magnitude of reduction in mEPSC amplitude is greater in *SynDIG4*$^{-/-}$ compared with *SynDIG1* mutant mice. Second, LTP induced by tetanic stimulation is abolished in both young and adult *SynDIG4*$^{-/-}$ mice, while mEPSC

amplitudes were reduced by 25% and basal fEPSP transmission was unchanged, which suggests an additional effect of SynDIG4 on synaptic plasticity beyond its role in synapse development. In contrast, such LTP is reduced only in young *SynDIG1* mutant mice, likely as a consequence of reduced synaptic transmission (Chenaux et al., 2016).

Altogether, our studies use a combination of approaches, including biochemistry, immunocytochemistry, electrophysiology, and behavior, to provide strong evidence that SynDIG4 establishes a pool of extrasynaptic AMPARs necessary for excitatory synapse development and function underlying higher-order cognitive plasticity.

EXPERIMENTAL PROCEDURES

Full experimental procedures are available in the Supplemental Information.

Animals

Frogs

Xenopus laevis frogs (females, age 1–3 years old) were used as the source for oocytes for heterologous expression and outside-out patch-clamp electrophysiological recordings. Maintenance of frogs and extraction of oocytes were performed in accordance with the NIH guidelines for the Care and Use of Laboratory Animals and Israeli law for animal experimentation and were approved by the Institutional Animal Care and Use Committee (IACUC) of the Hebrew University of Jerusalem.

Mice

The mutant allele [*Prrt1*$^{tm1(KOMP)Vlcg}$] was generated by Velocigene as part of KOMP and maintained on a C57BL/6 background. Mice (males and females) were used at the indicated ages for the following: biochemistry (P14), primary hippocampal culture (P1), electrophysiology (whole-cell patch-clamp, P12–P15; fEPSP, 8–12 weeks), and behavior (3–5 months). The use and maintenance of mice were carried out according to NIH guidelines and approved by the IACUC at University of California (UC), Davis.

Biochemical Fractionation and Quantitative Immunoblotting

The rostral two-thirds of P14 mouse brains were homogenized, and biochemical fractions were analyzed as described (Chenaux et al., 2016).

Primary Culture of Dissociated Hippocampal Neurons

Neurons from hippocampi of P1 WT and *SynDIG4*$^{-/-}$ littermates were dissociated individually in papain (Worthington) and plated (12,500 cells/cm^2) on poly-L-lysine-coated glass coverslips media supplemented with B-27 (Thermo Fisher Scientific). Neurons were analyzed as previously described (Kirk et al., 2016).

Electrophysiology

Intra- and extracellular recordings were performed using standard methods as previously described (Chenaux et al., 2016). Expression in *Xenopus laevis* oocytes and outside-out patch-clamp electrophysiological recordings were performed as described (Priel et al., 2006).

Mouse Behavior

Founder mice generated on the C57BL/6N background were backcrossed four times (N4) onto C57BL/6J to remove the *rd8* mutation (Mattapallil et al., 2012). Heterozygous N4 mice devoid of *rd8* were then intercrossed to produce WT and *SynDIG4*$^{-/-}$ mice.

Statistical Analyses

Data were analyzed in GraphPad Prism with the following statistical tests: two-tailed Student's t test (immunocytochemistry); one-way ANOVA (electrophysiology in oocytes); one-way ANOVA and Bonferroni's multiple comparison test (fEPSP), unpaired Student's t test (mEPSC). For the Morris water maze, latency was analyzed using two-way repeated-measures ANOVA with Bonferroni's post hoc tests. Probe trial data were analyzed using one-way ANOVA with Bonferroni post-tests. Novel object data were analyzed using paired Student's t test. All data are shown as mean ± SEM. Significance was *$p \leq 0.5$, **$p \leq 0.01$, and ***$p \leq 0.001$; NS indicates not significant.

SUPPLEMENTAL INFORMATION

Supplemental Information includes Supplemental Experimental Procedures, four figures, and four tables and can be found with this article online at https://doi.org/10.1016/j.celrep.2018.02.026.

ACKNOWLEDGMENTS

Funding was provided by the American Heart Association (11POST7020009 to L.M.), Brain & Behavior Research Foundation NARSAD Young Investigator (grant 20748 to L.M.), United States-Israel Binational Science Foundation (BSF; grant 2012781 to Y.S.-B.) and the United States National Science Foundation (NSF; grant 1322302 to E.D.), NIH (R01 MH097887 to J.W.H., R01 NS078792 to J.W.H., U54 HD079125 MCP to J.L.S. and J.N.C.) and NIH New Director's Innovator Award Program (DP2 OD006479-01 to E.D.), UC Davis Academic Senate Research Program Pilot Grant (to E.D.), and Whitehall Foundation (2015-05-106 to E.D.). L.M.K. is a trainee of the UC Davis MCB T32 Training Program (award GM007377). SynDIG4 KO mice were generated using the UC Davis Mouse Biology Program.

AUTHOR CONTRIBUTIONS

Methodology, L.M., L.M.K., G.C., Y.S.-B., J.N.C., J.W.H., and E.D.; Investigation, L.M., L.M.K., G.C., D.J.S., K.R.P., M.C.P., M.Q., T.H., and K.E.P.; Formal Analysis, L.M., L.M.K., G.C., D.J.S., M.Q., Y.S.-B., J.L.S., J.W.H., and E.D.; Writing, L.M., L.M.K., G.C., D.J.S., and E.D.; Funding Acquisition, L.M., Y.S.-B., J.W.H., and E.D.; Supervision, J.W.H. and E.D.

DECLARATION OF INTERESTS

The authors declare no competing interests.

Received: November 10, 2016
Revised: December 15, 2017
Accepted: February 6, 2018
Published: February 27, 2018

REFERENCES

Bourne, J.N., and Harris, K.M. (2011). Coordination of size and number of excitatory and inhibitory synapses results in a balanced structural plasticity along mature hippocampal CA1 dendrites during LTP. Hippocampus *21*, 354–373.

Brielmaier, J., Matteson, P.G., Silverman, J.L., Senerth, J.M., Kelly, S., Genestine, M., Millonig, J.H., DiCicco-Bloom, E., and Crawley, J.N. (2012). Autism-relevant social abnormalities and cognitive deficits in engrailed-2 knockout mice. PLoS ONE *7*, e40914.

Chen, L., Chetkovich, D.M., Petralia, R.S., Sweeney, N.T., Kawasaki, Y., Wenthold, R.J., Bredt, D.S., and Nicoll, R.A. (2000). Stargazin regulates synaptic targeting of AMPA receptors by two distinct mechanisms. Nature *408*, 936–943.

Chen, N., Pandya, N.J., Koopmans, F., Castelo-Székelv, V., van der Schors, R.C., Smit, A.B., and Li, K.W. (2014). Interaction proteomics reveals brain region-specific AMPA receptor complexes. J. Proteome Res. *13*, 5695–5706.

Chenaux, G., Matt, L., Hill, T.C., Kaur, I., Liu, X.B., Kirk, L.M., Speca, D.J., McMahon, S.A., Zito, K., Hell, J.W., and Díaz, E. (2016). Loss of SynDIG1 reduces excitatory synapse maturation but not formation *in vivo*. eNeuro *3*, ENEURO.0130-16.2016.

Cohen, S.J., Munchow, A.H., Rios, L.M., Zhang, G., Asgeirsdóttir, H.N., and Stackman, R.W., Jr. (2013). The rodent hippocampus is essential for nonspatial object memory. Curr. Biol. *23*, 1685–1690.

Díaz, E. (2010). Regulation of AMPA receptors by transmembrane accessory proteins. Eur. J. Neurosci. *32*, 261–268.

Erlenhardt, N., Yu, H., Abiraman, K., Yamasaki, T., Wadiche, J.I., Tomita, S., and Bredt, D.S. (2016). Porcupine controls hippocampal AMPAR levels, composition, and synaptic transmission. Cell Rep. *14*, 782–794.

Granger, A.J., Shi, Y., Lu, W., Cerpas, M., and Nicoll, R.A. (2013). LTP requires a reserve pool of glutamate receptors independent of subunit type. Nature *493*, 495–500.

Huganir, R.L., and Nicoll, R.A. (2013). AMPARs and synaptic plasticity: the last 25 years. Neuron *80*, 704–717.

Jackson, A.C., and Nicoll, R.A. (2011). The expanding social network of ionotropic glutamate receptors: TARPs and other transmembrane auxiliary subunits. Neuron *70*, 178–199.

Jordan, B.A., Fernholz, B.D., Boussac, M., Xu, C., Grigorean, G., Ziff, E.B., and Neubert, T.A. (2004). Identification and verification of novel rodent postsynaptic density proteins. Mol. Cell. Proteomics *3*, 857–871.

Kalashnikova, E., Lorca, R.A., Kaur, I., Barisone, G.A., Li, B., Ishimaru, T., Trimmer, J.S., Mohapatra, D.P., and Díaz, E. (2010). SynDIG1: an activity-regulated, AMPA- receptor-interacting transmembrane protein that regulates excitatory synapse development. Neuron *65*, 80–93.

Kapus, G., Székely, J.I., Durand, J., Ruiz, A., and Tarnawa, I. (2000). AMPA receptor antagonists, GYKI 52466 and NBQX, do not block the induction of long-term potentiation at therapeutically relevant concentrations. Brain Res. Bull. *52*, 511–517.

Kaur, I., Yarov-Yarovoy, V., Kirk, L.M., Plambeck, K.E., Barragan, E.V., Ontiveros, E.S., and Díaz, E. (2016). Activity-dependent palmitoylation controls SynDIG1 stability, localization, and function. J. Neurosci. *36*, 7562–7568.

Kirk, L.M., Ti, S.W., Bishop, H.I., Orozco-Llamas, M., Pham, M., Trimmer, J.S., and Díaz, E. (2016). Distribution of the SynDIG4/proline-rich transmembrane protein 1 in rat brain. J. Comp. Neurol. *524*, 2266–2280.

Lee, K.F., Soares, C., and Béïque, J.C. (2014). Tuning into diversity of homeostatic synaptic plasticity. Neuropharmacology *78*, 31–37.

Lovero, K.L., Blankenship, S.M., Shi, Y., and Nicoll, R.A. (2013). SynDIG1 promotes excitatory synaptogenesis independent of AMPA receptor trafficking and biophysical regulation. PLoS ONE *8*, e66171.

Lu, W., Shi, Y., Jackson, A.C., Bjorgan, K., During, M.J., Sprengel, R., Seeburg, P.H., and Nicoll, R.A. (2009). Subunit composition of synaptic AMPA receptors revealed by a single-cell genetic approach. Neuron *62*, 254–268.

Mattapallil, M.J., Wawrousek, E.F., Chan, C.C., Zhao, H., Roychoudhury, J., Ferguson, T.A., and Caspi, R.R. (2012). The Rd8 mutation of the Crb1 gene is present in vendor lines of C57BL/6N mice and embryonic stem cells, and confounds ocular induced mutant phenotypes. Invest. Ophthalmol. Vis. Sci. *53*, 2921–2927.

Park, J., Chávez, A.E., Mineur, Y.S., Morimoto-Tomita, M., Lutzu, S., Kim, K.S., Picciotto, M.R., Castillo, P.E., and Tomita, S. (2016). CaMKII phosphorylation of TARPγ-8 is a mediator of LTP and learning and memory. Neuron *92*, 75–83.

Priel, A., Selak, S., Lerma, J., and Stern-Bach, Y. (2006). Block of kainate receptor desensitization uncovers a key trafficking checkpoint. Neuron *52*, 1037–1046.

Romberg, C., Raffel, J., Martin, L., Sprengel, R., Seeburg, P.H., Rawlins, J.N., Bannerman, D.M., and Paulsen, O. (2009). Induction and expression of GluA1 (GluR-A)-independent LTP in the hippocampus. Eur. J. Neurosci. *29*, 1141–1152.

Sällman Almén, M., Bringeland, N., Fredriksson, R., and Schiöth, H.B. (2012). The dispanins: a novel gene family of ancient origin that contains 14 human members. PLoS ONE *7*, e31961.

Schwenk, J., Harmel, N., Zolles, G., Bildl, W., Kulik, A., Heimrich, B., Chisaka, O., Jonas, P., Schulte, U., Fakler, B., and Klöcker, N. (2009). Functional proteomics identify cornichon proteins as auxiliary subunits of AMPA receptors. Science *323*, 1313–1319.

Schwenk, J., Harmel, N., Brechet, A., Zolles, G., Berkefeld, H., Müller, C.S., Bildl, W., Baehrens, D., Hüber, B., Kulik, A., et al. (2012). High-resolution proteomics unravel architecture and molecular diversity of native AMPA receptor complexes. Neuron *74*, 621–633.

Schwenk, J., Baehrens, D., Haupt, A., Bildl, W., Boudkkazi, S., Roeper, J., Fakler, B., and Schulte, U. (2014). Regional diversity and developmental dynamics of the AMPA-receptor proteome in the mammalian brain. Neuron *84*, 41–54.

Shanks, N.F., Savas, J.N., Maruo, T., Cais, O., Hirao, A., Oe, S., Ghosh, A., Noda, Y., Greger, I.H., Yates, J.R., 3rd, and Nakagawa, T. (2012). Differences in AMPA and kainate receptor interactomes facilitate identification of AMPA receptor auxiliary subunit GSG1L. Cell Rep. *1*, 590–598.

Sumioka, A., Brown, T.E., Kato, A.S., Bredt, D.S., Kauer, J.A., and Tomita, S. (2011). PDZ binding of TARPγ-8 controls synaptic transmission but not synaptic plasticity. Nat. Neurosci. *14*, 1410–1412.

Tomita, S., Chen, L., Kawasaki, Y., Petralia, R.S., Wenthold, R.J., Nicoll, R.A., and Bredt, D.S. (2003). Functional studies and distribution define a family of transmembrane AMPA receptor regulatory proteins. J. Cell Biol. *161*, 805–816.

Turrigiano, G.G. (2008). The self-tuning neuron: synaptic scaling of excitatory synapses. Cell *135*, 422–435.

Turrigiano, G. (2012). Homeostatic synaptic plasticity: local and global mechanisms for stabilizing neuronal function. Cold Spring Harb. Perspect. Biol. *4*, a005736.

Valente, P., Castroflorio, E., Rossi, P., Fadda, M., Sterlini, B., Cervigni, R.I., Prestigio, C., Giovedì, S., Onofri, F., Mura, E., et al. (2016). PRRT2 is a key component of the Ca(2+)-dependent neurotransmitter release machinery. Cell Rep. *15*, 117–131.

Valenzuela, D.M., Murphy, A.J., Frendewey, D., Gale, N.W., Economides, A.N., Auerbach, W., Poueymirou, W.T., Adams, N.C., Rojas, J., Yasenchak, J., et al. (2001). High-throughput engineering of the mouse genome coupled with high-resolution expression analysis. Nat. Biotechnol. *21*, 652–659.

Vogel-Ciernia, A., and Wood, M.A. (2014). Examining object location and object recognition memory in mice. Curr. Protoc. Neurosci. *69*, 8.31:8.31.1–8.31.17.

von Engelhardt, J., Mack, V., Sprengel, R., Kavenstock, N., Li, K.W., Stern-Bach, Y., Smit, A.B., Seeburg, P.H., and Monyer, H. (2010). CKAMP44: a brain-specific protein attenuating short-term synaptic plasticity in the dentate gyrus. Science *327*, 1518–1522.

Yang, M., Lewis, F.C., Sarvi, M.S., Foley, G.M., and Crawley, J.N. (2015). 16p11.2 deletion mice display cognitive deficits in touchscreen learning and novelty recognition tasks. Learn. Mem. *22*, 622–632.

Cell Reports, Volume *22*

Supplemental Information

SynDIG4/Prrt1 Is Required for Excitatory Synapse Development and Plasticity Underlying Cognitive Function

Lucas Matt, Lyndsey M. Kirk, George Chenaux, David J. Speca, Kyle R. Puhger, Michael C. Pride, Mohammad Qneibi, Tomer Haham, Kristopher E. Plambeck, Yael Stern-Bach, Jill L. Silverman, Jacqueline N. Crawley, Johannes W. Hell, and Elva Díaz

SUPPLEMENTAL FIGURES AND LEGENDS

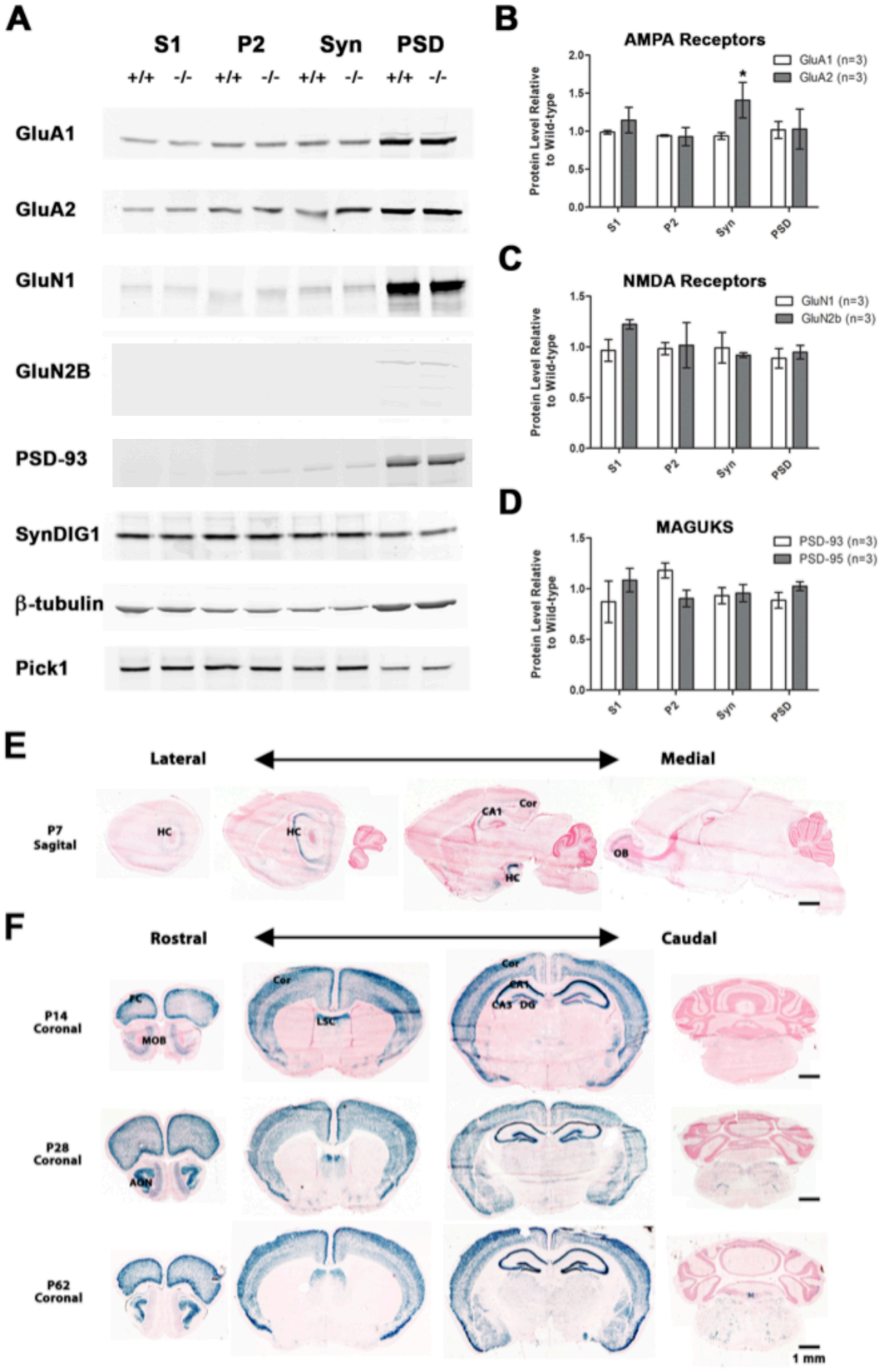

Figure S1. SynDIG4 deficient synapses have unchanged relative protein levels, Related to Figure 2.

(A) Representative immunoblots of biochemical fractions (10 µg protein loaded per lane) isolated from wild-type (+/+) and *SynDIG4*$^{-/-}$ homozygous mutant P14 mouse brain tissue showing levels of GluA1, GluA2, GluN1, GluN2B, PSD-93, SynDIG1, β-tubulin, and Pick-1 present in the postnuclear supernatant (S1), membrane pellet (P2), synaptosomal (Syn), and postsynaptic density (PSD) enriched fractions.

(B-D) Bar charts depicting the ratio of *SynDIG4*$^{-/-}$ homozygous mutant protein relative to wild-type levels of AMPA receptor subunits (B), NMDA receptor subunits (C), and PSD-93 and PSD-95 (D) in the PSD enriched fractions. Data are the average of three independent biochemical fractionation experiments; each experiment utilized 4-6 mouse forebrains of each genotype. Similar results were obtained with adult *SynDIG4*$^{-/-}$ and WT littermates (not shown). Error bars, ± standard error of the mean (SEM). Significance is indicated as: $*p < 0.05$.

(E) Sagittal sections from P7 *SynDIG4*$^{-/-}$ mice show β-gal reporter activity (blue) in the CA1 region of the hippocampus (HC) and within the olfactory bulb (OB).

(F) Coronal sections of P14, P28, and P62 mutant mouse brains show β-gal expression in frontal cortex (FC), main olfactory bulb (MOB), neocortex (Cor), caudal portion of the lateral septal nucleus (LSC), anterior olfactory nucleus (AON), and CA1, CA3, and dentate gyrus (DG) regions within the hippocampus.

All sections are counterstained with nuclear fast red. Some images are composites combining multiple individual images into one apparent photograph. Scale bar, 1 mm.

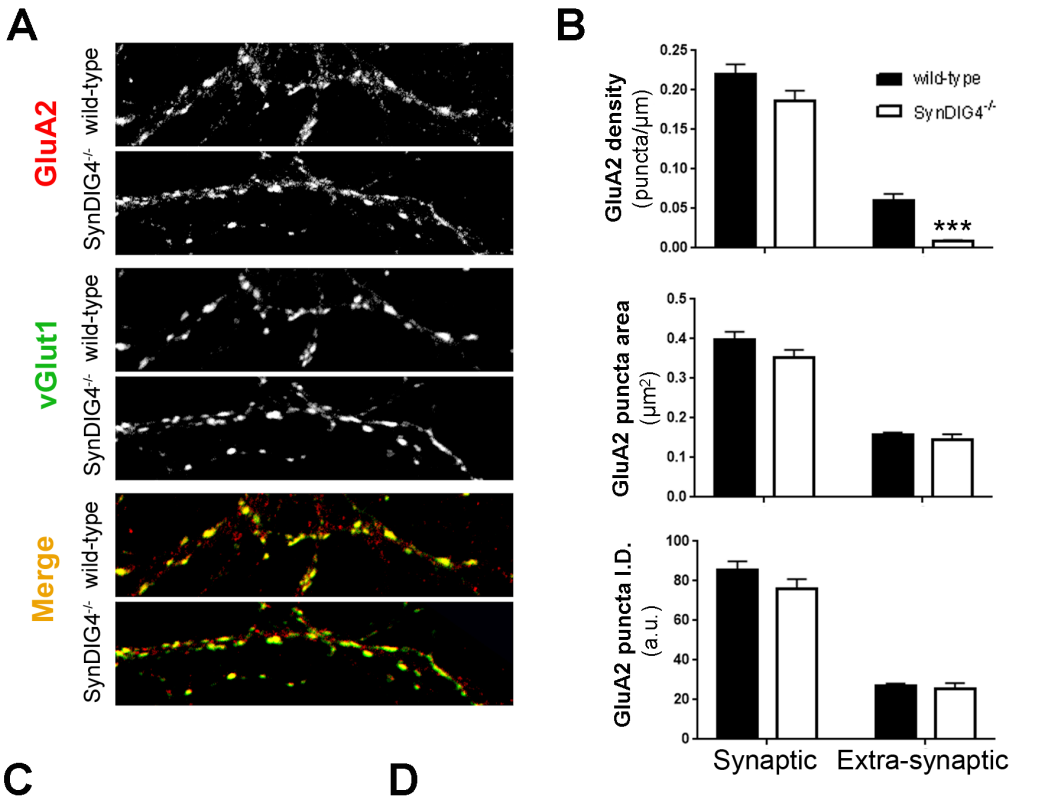
A
GluA2
vGlut1
Merge
wild-type
SynDIG4-/-
B
GluA2 density (puncta/µm)
wild-type
SynDIG4-/-
***
GluA2 puncta area (µm2)
GluA2 puncta I.D. (a.u.)
Synaptic
Extra-synaptic

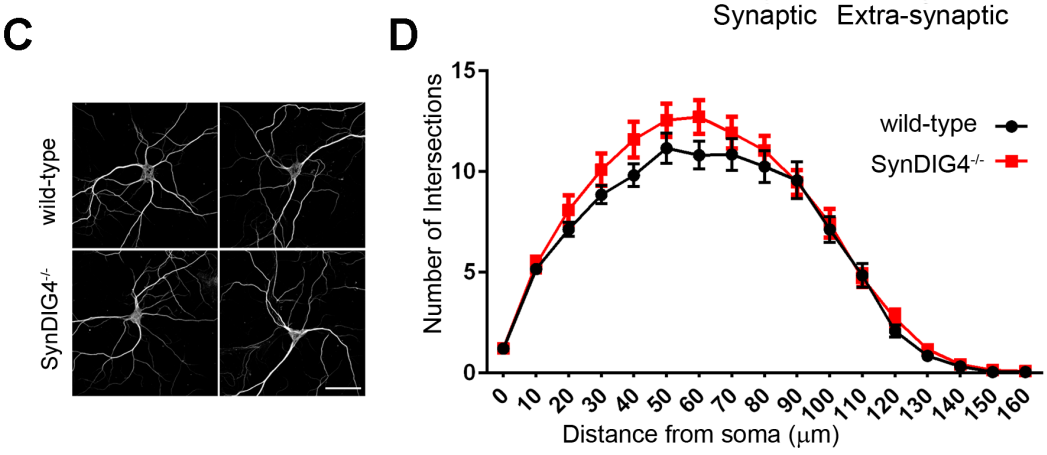
C
wild-type
SynDIG4-/-
D
Number of Intersections
wild-type
SynDIG4-/-
Distance from soma (µm)

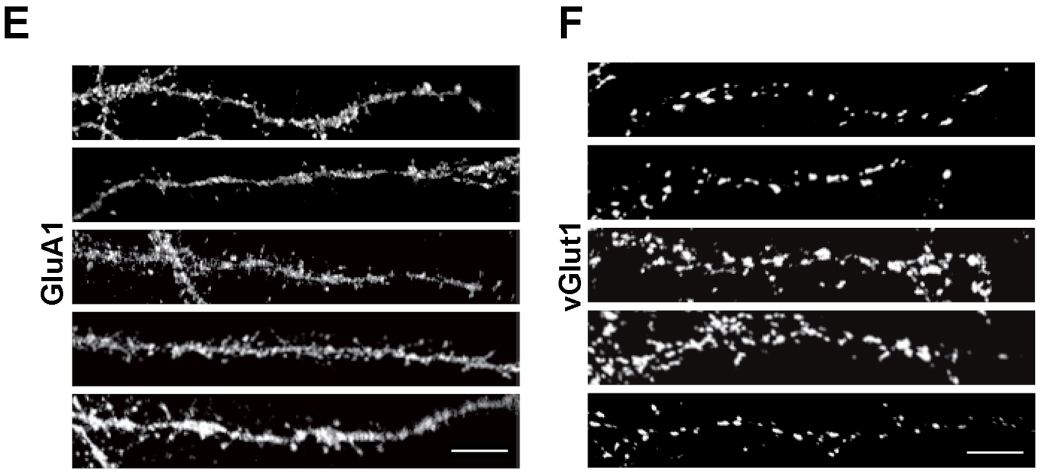
E
GluA1
F
vGlut1

Figure S2. Loss of SynDIG4 has no significant effect on synaptic GluA2 or dendrite complexity, Related to Figure 2.

(A) Representative images of wild-type and *SynDIG4*$^{-/-}$ dissociated hippocampal neurons at 14 DIV, stained with GluA2 and vGlut1.

(B) Graphs depict quantification of synaptic (overlap with vGlut1) or extrasynaptic (no overlap with vGlut1) GluA2 puncta density, puncta size and puncta Integrated Density (I.D.); Data are averaged from two independent experiments; n = 24-25 cells per genotype, per experiment; three dendrites per cell were selected for analysis.

(C) Representative neurons used in Sholl analysis stained with antibody against Map2b. Scale bar = 50 μm.

(D) Sholl analysis shows no significant difference in dendrite complexity (measured as the number of intersections at a defined radius from the soma) in wild-type vs *SynDIG4*$^{-/-}$ neurons.

(E-F) Representative dendritic stretches of dissociated rat hippocampal neurons at 14 DIV, stained separately for either GluA1 (E) or vGlut1 (F) and Alexa488- and Cy5-conjugated secondary antibodies. Note that GluA1 immunostaining is both punctate and diffuse, and can be clearly visualized in both dendritic spines and shafts while vGlut1 immunostaining labels distinct punctate structures in contact with the dendritic shaft, indicative of a pre-synaptic input. Five representative dendrite stretches were chosen from 10 different cells per condition/staining. Scale bar = 10 μm.

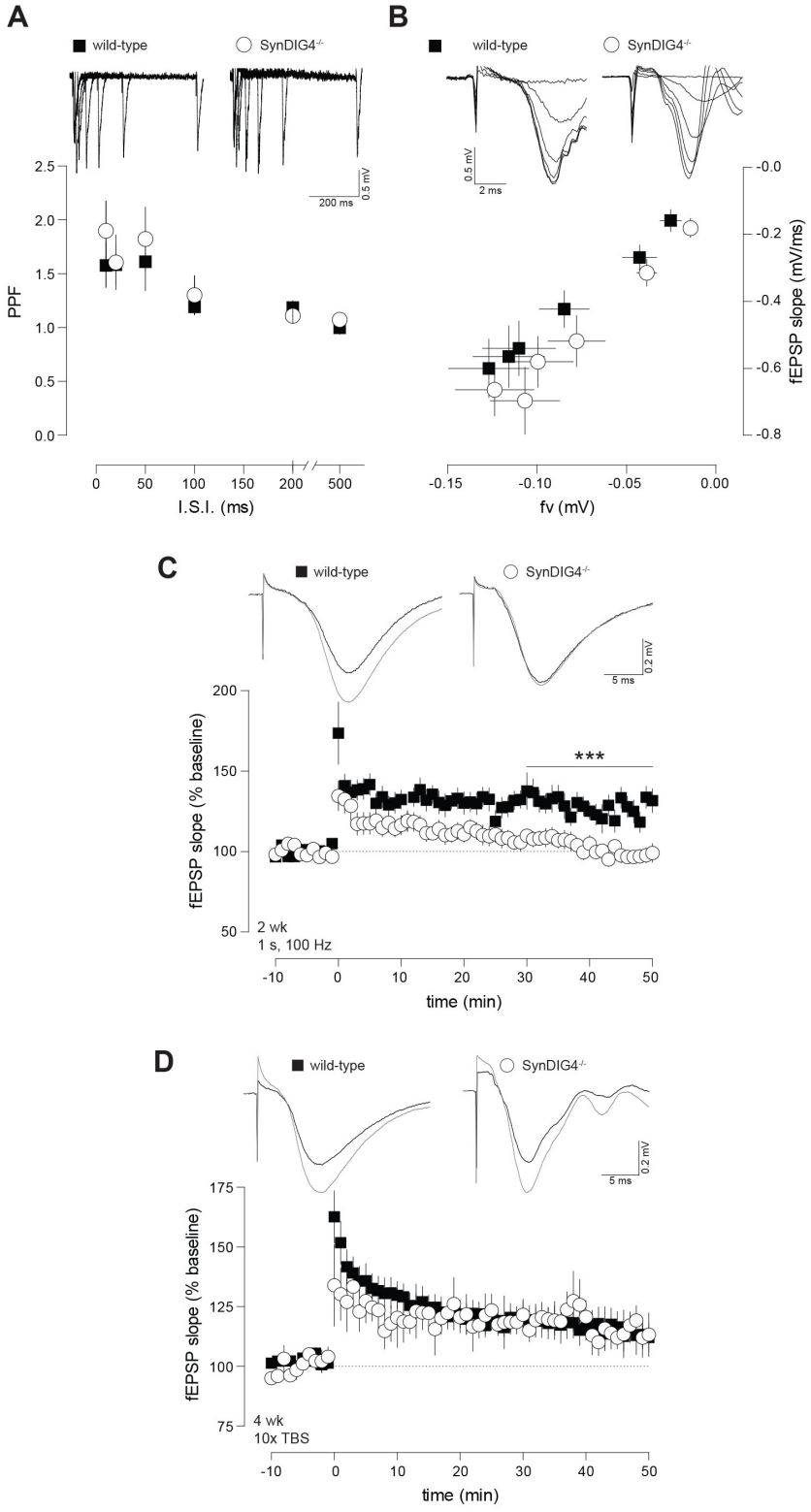
A
wild-type
SynDIG4-/-
200 ms
0.5 mV
PPF
I.S.I. (ms)
B
wild-type
SynDIG4-/-
0.5 mV
2 ms
fEPSP slope (mV/ms)
fv (mV)
C
wild-type
SynDIG4-/-
0.2 mV
5 ms
fEPSP slope (% baseline)
***
2 wk
1 s, 100 Hz
time (min)
D
wild-type
SynDIG4-/-
0.2 mV
5 ms
fEPSP slope (% baseline)
4 wk
10x TBS
time (min)

Figure S3. Synaptic transmission and plasticity properties in *SynDIG4*$^{-/-}$ mice, Related to Figure 3.

(A-B) Schaffer-collateral fEPSP were recorded from acute forebrain slices of 8 – 12 week-old wild-type and *SynDIG4*$^{-/-}$ mice.

(A) Paired-pulse facilitation (PPF) was not different between wild-type (n = 15) and *SynDIG4*$^{-/-}$ (n = 16) for all inter-stimulus intervals (I.S.I.). Traces from representative recordings shown on top (wild-type: 10 ms: 1.6 ± 0.2 mV, 20 ms: 1.6 ± 0.2 mV, 50 ms: 1.6 ± 0.3 mV, 100 ms: 1.2 ± 0.1 mV, 200 ms: 1.2 ± 0.1 mV, 500 ms: 1.0 ± 0.1 mV, n = 15; SynDIG4$^{-/-}$: 10 ms: 1.9 ± 0.3 mV, 20 ms: 1.6 ± 0.3 mV, 50 ms: 1.8 ± 0.3 mV, 100 ms: 1.3 ± 0.2 mV, 200 ms: 1.1 ± 0.1 mV, 500 ms: 1.1 ± 0.1 mV, n = 16).

(B) Averaged fEPSP slope was plotted against averaged fiber volley amplitude (fv) for all signals elicited by increasing stimulation strengths. No difference was observed between wild-type (-0.025 ± 0.006 mV / -0.16 ± 0.03 mV/ms, -0.043 ± 0.010 mV / -0.27 ± 0.04 mV/ms, -0.085 ± 0.014 mV / -0.42 ± 0.05 mV/ms, -0.110 ± 0.020 mV / -0.54 ± 0.08 mV/ms, -0.116 ± 0.020 mV / -0.56 ± 0.09 mV/ms, -0.127 ± 0.022 mV / -0.60 ± 0.09 mV/ms ;n = 14) and *SynDIG4*$^{-/-}$ (-0.014 ± 0.003 mV / -0.18 ± 0.03 mV/ms, -0.039 ± 0.006 mV/ -0.18 ± 0.03 mV/ms, -0.078 ± 0.016 mV / -0.52 ± 0.08 mV/ms, -0.100 ± 0.020 mV / -0.58 ± 0.08 mV/ms, -0.107 ± 0.019 mV / -0.70 ± 0.10 mV/ms, -0.124 ± 0.022 mV, -0.66 ± 0.08 mV/ms; n = 8).

(C) Schaffer-collateral fEPSP were recorded from acute forebrain slices of two week-old mice. The 1 sec, 100 Hz tetanus elicits robust LTP in wild-type but not *SynDIG4*$^{-/-}$ mice (wild-type: 128 ± 7, n = 10, $p < 0.001$ vs baseline; *SynDIG4*$^{-/-}$: 100 ± 4, n = 15, $p < 0.001$ vs WT; 1-way ANOVA with Bonferroni's Test between baseline and tetanized and between tetanized).

(**D**) Schaffer-collateral fEPSP were recorded from acute forebrain slices of 4 week-old mice. Theta-burst stimulus (TBS) led to robust LTP in *SynDIG4*$^{-/-}$ mice not different from control (wild-type: 115 ± 6, n = 5, $p < 0.05$ t-test vs baseline; *SynDIG4*$^{-/-}$: 115 ± 6, n = 4, $p < 0.001$ t-test vs baseline).

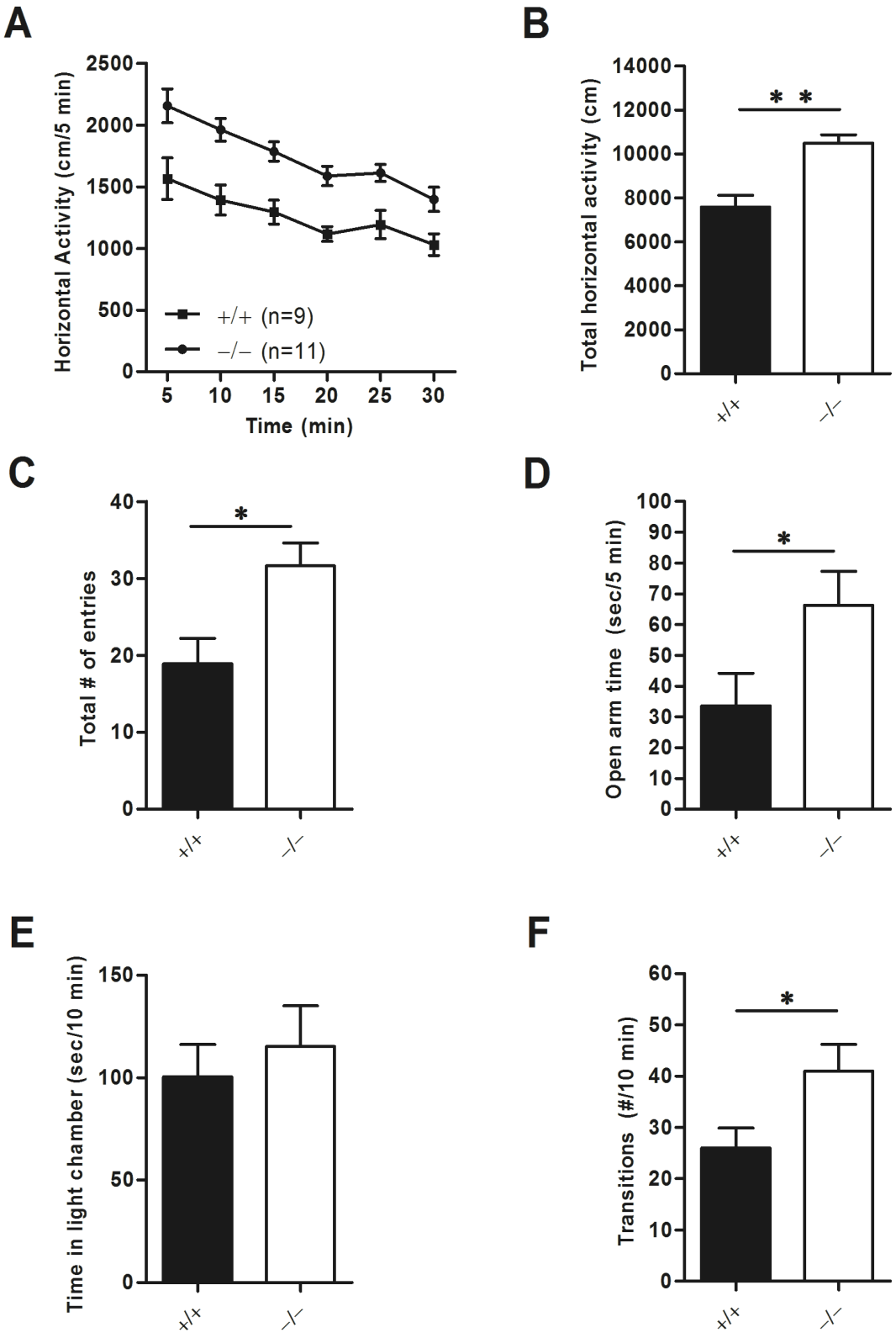
A
Horizontal Activity (cm/5 min)
2500
2000
1500
1000
500
0
+/+ (n=9)
–/– (n=11)
5
10
15
20
25
30
Time (min)
B
Total horizontal activity (cm)
14000
12000
10000
8000
6000
4000
2000
0
* *
+/+
–/–
C
Total # of entries
40
30
20
10
0
*
+/+
–/–
D
Open arm time (sec/5 min)
100
90
80
70
60
50
40
30
20
10
0
*
+/+
–/–
E
Time in light chamber (sec/10 min)
150
100
50
0
+/+
–/–
F
Transitions (#/10 min)
60
50
40
30
20
10
0
*
+/+
–/–

Figure S4. Additional behavioral phenotypes of *SynDIG4*$^{-/-}$ mice, Related to Figure 4.

(A) Locomotor activity of *SynDIG4*$^{-/-}$ mice is significantly higher than wild-type mice.

(B) Total horizontal distance traveled in (A) is significantly higher in *SynDIG4*$^{-/-}$ mice than wild-type mice.

(C) In the elevated plus-maze (EPM), the total number of entries is significantly higher in *SynDIG4*$^{-/-}$ mice than wild-type mice.

(D) Time spent in the open arms of the EPM is significantly higher in *SynDIG4*$^{-/-}$ mice than wild-type mice.

(E) In the light↔dark (L↔D) box, the time spent in the light chamber did not differ between *SynDIG4*$^{-/-}$ mice and wild-type mice.

(F) In the L↔D box, the number of transitions was significantly higher in *SynDIG4*$^{-/-}$ mice than wild-type mice.

The significant differences observed in the EPM and L↔D tests could be a consequence of the elevated exploratory locomotor activity of the *SynDIG4*$^{-/-}$ animals.

For all experiments: wild-type, n = 9; *SynDIG4*$^{-/-}$, n = 11; Significance is indicated as: *$p < 0.05$; **$p < 0.01$.

SUPPLEMENTAL TABLES

Table S2. Primary Antibody Information, Related to Figures 2, S1, S2.

Target	Source	Catalog #	Species	Figure
β-actin	Abcam	ab8224	rabbit polyclonal	2
β-tubulin	Millipore	05-661	mouse monoclonal	S1
GluA1	Millipore	AB1504	rabbit polyclonal	2, S1
GluA2	NeuroMab	75-002	mouse monoclonal	S1, S2
GluN1	BD Biosciences	556308	mouse monoclonal	S1
GluN2B	NeuroMab	75-097	mouse monoclonal	S1
Map2b	Sigma	M4403	mouse monoclonal	S2
Pick1	NeuroMab	73-040	mouse monoclonal	S1
PSD-93	NeuroMab	75-057	mouse monoclonal	S1
PSD-95	NeuroMab	75-028	mouse monoclonal	2
Synaptophysin	Synaptic Systems	101011	mouse monoclonal	2
SynDIG1	NeuroMab	75-251	mouse monoclonal	S1
SynDIG4 (NG5.1)	Gift from A.B. Smit	custom	rabbit polyclonal	2
vGlut1	Millipore	AB5905	guinea pig polyclonal	2, S2

Table S3. Level and area of total GluA1 and GluA2 that does not overlap with vGlut1, Related to Figure 2.

	genotype	results	n	Statistics
		Total GluA1 per µm dendrite	Cells, dendrites	
	wild-type	Summed levels: 404.29±32 Summed area: 0.0336±0.0026	25,125	
	SynDIG4$^{-/-}$	Summed levels: 205.43±18 Summed area: 0.0177±0.0015	25,125	p = 2.2141E-07 vs wild-type p = 4.4082E-07 vs wild-type
		Total GluA2 per µm dendrite	Cells, dendrites	
	wild-type	Summed levels: 520.10±50.21 Summed area: 0.0313±0.003	25, 69	
	SynDIG4$^{-/-}$	Summed levels: 211.23±20.69 Summed area: 0.0123±0.001	25, 74	p = 1.5619E-07 vs wild-type p = 4.7565E-08 vs wild-type

Table S4. General health information for *SynDIG4*$^{-/-}$ and WT mice, Related to Figure 4.

Genotypes	**WT** N = 9	***SynDIG4* -/-** N = 11	***p*-value**
Body Weight	26.68±1.54	23.1±2.3	not significant (n.s.)
Body Temperature	36.34±0.23	36.38±0.168	n.s.
Fur quality (3 pt scale)	2	2	n.s.
Bald patches (%)	0%	0%	n.s.
Missing whiskers (%)	0%	0%	n.s.
Piloerection	0%	0%	n.s.
Body tone (3 pt scale)	2	2	n.s.
Limb tone (3 pt scale)	2	2	n.s.
Skin color (3 pt scale)	2	2	n.s.
Physical abnormalities	0%	0%	n.s.
Trunk curl (%)	100%	100%	n.s.
Wire hang (sec)	60±0	60±0	n.s.
Forepaw reach (%)	100%	100%	n.s.
Righting reflex (%)	100%	100%	n.s.
Corneal (%)	100%	100%	n.s.
Whisker twitch (%)	100%	100%	n.s.
Ear twitch (%)	100%	100%	n.s.
Auditory startle (%)	100%	100%	n.s.
Struggle/vocalization (%)	33.33%	18.18%	n.s.
Dowel biting (3 pt scale)	2.33	2.27	n.s.

EXPERIMENTAL PROCEDURES

Animals

Frogs. Xenopus laevis frogs (females, age 1-3 years old) were used as a source for oocytes for heterologous expression and outside-out patch-clamp electrophysiological recordings. Maintenance of the frogs and extraction of oocytes were performed in accordance with the National Institutes of Health (NIH) guidelines for the Care and Use of Laboratory Animals and the Israeli law for animal experimentation and were approved by the Institutional Animal Care and Use Committee (IACUC) of the Hebrew University of Jerusalem.

Mice. Mouse embryonic stem (ES) cells with a targeted deletion of the SynDIG4 locus were obtained from the Mouse Biology Program (MBP) at UC Davis. The mutant allele [*Prrt1*$^{tm1(KOMP)Vlcg}$] was generated by Velocigene as part of the trans-NIH Knock Out Mouse Project (KOMP), obtained from the KOMP Repository (www.komp.org) and maintained on C57BL/6 line. NIH grants to Velocigene at Regeneron Inc (U01HG004085) and the CSD Consortium (U01HG004080) funded the generation of gene-targeted ES cells for 8500 genes in the KOMP Program and archived and distributed by the KOMP Repository at UC Davis and CHORI (U42RR024244). The β-galactosidase (β-gal) and neomycin cassette ZEN-UB1 replaced the protein coding region of the *SynDIG4* locus leaving non-coding portions of exons 1 and 4 and β-gal expression driven by the SynDIG4 promoter. The day of birth is referred to as postnatal day 0 (P0). Wild-type (WT) controls are either littermates or are derived from separate homozygous crosses from a common lineage. Mutant mice are viable and fertile, exhibit Mendelian inheritance and do not exhibit any alterations in parameters of general health (Table S6). All mice were group-housed in a climate-controlled facility on a 12-hour light/dark cycle (lights on at 06:00), and food (Teklad 2918, Harlan) and water were available *ad libitum*. Corncob bedding with a handful of shredded paper and nestlets (Eco-Bedding™, FiberCore, Cleveland, OH) lined the cage bottom. *Rats.* Sprague Dawley timed pregnant rats were

purchased from Harlan. Rats were housed and maintained in the animal facility at UC Davis. The use and maintenance of animals were carried out according to the guidelines set forth by the NIH and approved by IACUC at UC Davis.

Antibodies and Reagents

All primary antibodies used in the present study are listed in Table S1. The following secondary antibodies were used: Alexa Fluor 488-conjugated secondary antibodies (Molecular Probes), Cy3- or Cy5-conjugated secondary antibodies (Jackson ImmunoResearch), IRDye-conjugated secondary antibodies (LiCOR), and HRP-conjugated secondary antibodies (Thermo Fisher Scientific).

PSD fractionation and immunoblotting

The rostral 2/3 of P14 mouse brains were homogenized by dounce homogenation in 0.32 M sucrose, 1 mM Tris pH 7.4, 1 mM $MgCl_2$ with protease inhibitors (leupeptin, aprotinin, pepstatin A, and phenylmethylsulfonyl fluoride). Lysate was spun 15 minutes at 1400 xg. Supernatant was collected and saved. The pellet was homogenized with more sucrose solution and large insoluble debris and the nuclear fraction were removed by centrifugation at 710 xg. The supernatants were pooled and an aliquot saved as the postnuclear supernatant (S1) fraction. The remaining S1 was centrifuged at 16000 xg, and the pellet collected as the membrane-enriched fraction (P2). The P2 fraction was resuspended in 0.32 M sucrose solution without $MgCl_2$ and layered over 0.85 M, 1.0 M, and 1.25 M sucrose gradients, spun at 40000 xg for 2 hours, and synaptosomal enriched fraction (Syn) was collected between 1.0/1.25 M gradients. Triton X-100 was added to Syn to a final concentration of 0.5% and incubated for 15 minutes at 4°C. The pellet was collected after 100000 xg spin for 30 minutes. The pellet was resuspended in sucrose buffer, placed over another sucrose gradient (1.0/1.5/2.0 M), centrifuged at 40000 xg for 2 hours, and second gradient layer collected between 1.5/2.0 M sucrose interface. This

fraction was exposed to Triton X-100 again and a final PSD pellet collected after centrifugation at 100000 xg for 1 hour, which was resuspended via sonication to obtain the PSD enriched fraction (PSD). Protein was quantified using a BCA assay (Thermo Fisher Scientific) and 10-20 μg of protein were run on 7-15% acrylamide gels, which were transferred to nitrocellulose membranes, stained with antibodies, and protein levels measured on an Odyssey® LICOR system. S1, P2, Syn and PSD fractions were normalized to β-actin and/or β-tubulin. *SynDIG4*$^{-/-}$ mutant fractions were divided by WT protein levels and student's t-test analyses revealed no statistically significant differences.

X-gal staining

Unfixed fresh mouse brains (ages P7, P14, P28, P62) were quickly frozen on dry ice in Optimal Cutting Temperature (OCT) medium and sectioned at 15-25 μm on a Leica cryostat. Sections were stained with X-gal (5-Bromo-4-chloro-3-indolyl-β-D-galactopyranoside; Roche).

Primary dissociated neuronal culture and Immunocytochemistry

Cell culture and Immunocytochemistry. Neurons from hippocampi of P1 WT and *SynDIG4*$^{-/-}$ mice littermates were dissociated individually in papain (Worthington) and plated at a density of 12,500 cells/cm^2. Neurons from hippocampi of embryonic day 18 (E18) WT rat embryos were dissociated with 2.5% trypsin (Life Technologies) and plated at a density of 5,500/cm^2. Neurons were grown on poly-L-lysine-coated glass coverslips media supplemented with B-27 and N2 (Thermo Fisher Scientific). Neurons were fixed in 4% formaldehyde at 14 days in vitro (DIV), permeabilized for 15 min in 0.1% Triton X-100, and blocked for 30 min in 3-10% bovine serum albumin (Life Technologies). Coverslips were incubated in primary antibody overnight at 4°C, secondary antibody at room temperature (RT) for 1 hr, and mounted onto glass slides using Flouromount-G (Southern Biotech).

Image acquisition. Images were acquired using a Zeiss LSM700 scanning confocal microscope or an Olympus Fluoview 1000, with a 63x/ 1.5 NA objective with identical settings for laser power, photomultiplier gain, and digital offset within each experiment. Settings were established such that no signal was observed with coverslips stained only with secondary antibodies. Imaging was performed blinded as to genotype.

Image analysis. All analyses were performed blind to genotype. Images were imported into ImageJ software for identification of representative stretches for quantitative analysis of synaptic puncta (colocalized with vGlut1) or extrasynaptic puncta (no colocalization with vGlut1), and addition of scale bars. Thresholds were established using a subset of images from each image set so that all puncta were included, and the average threshold was applied to the entire data set for quantitative analysis. A minimum size cutoff of 0.09 was applied to eliminate speckled background stain. For each cell, dendrites beyond the first branch point were selected for quantification. A mask was created for each channel, and colocalization was defined as any partially overlapping punctate structure. Synaptic AMPARs were identified as puncta colocalizing with vGlut1. Another mask was then created of the synaptic puncta, and was subtracted from the mask of total AMPAR puncta to create a mask representing "extrasynaptic AMPARs." These masks were used to measure puncta size and number of puncta, and were redirected to the original image for fluorescence quantification (Integrated Density, I.D.). Density was calculated by measuring the number of puncta per length of dendrite. For extrasynaptic levels and area, images were thresholded as described above. A mask was created for synapses (identified by the overlap of GluA and vGlut1 staining) and subtracted from the GluA image, leaving only extra-synaptic signal. No size cutoff was applied; therefore, all particles that passed the threshold were included in the analysis. The total greyscale levels and area were summed for the dendrite stretch, and normalized to dendrite length. Data were imported into GraphPad Prism 7.0 for statistical analysis and a two-tailed student's t-test was calculated. All data are shown as mean ± standard error of the mean (SEM). Significance levels are indicated

by asterisks: * $p \leq 0.5$, ** $p \leq 0.01$, *** $p \leq 0.001$. Signals were adjusted for all images by using linear adjustments of levels in Photoshop and figures assembled in Illustrator (Adobe Systems). All panels within a figure were treated identically. Data are presented as mean ± SEM.

Sholl analysis. The morphometric Sholl analysis was obtained from WT and *SynDIG4*$^{-/-}$ dissociated hippocampal neurons fixed and stained at 14 DIV with Map2b primary antibody. Dendrites were traced using the Fiji extension Simple Neurite Tracer, followed by Sholl analysis plugin. A series of concentric spheres (centered around the soma) were drawn with an intersection interval of 10 μm and the number of dendrites crossing each sphere was calculated and was plotted against the distance from the soma.

Statistical analysis. GraphPad Prism was used to calculate a repeated measure ANOVA with genotype as the between group factor and distance from soma as the repeated measure factor. Holm-Sidak multiple comparison test was used to compare means of a defined distance to soma between different genotypes. All tracings and analyses were blinded to genotype. Data are presented as mean ± SEM.

Electrophysiology

Heterologous expression in oocytes and outside-out patch-clamp recordings. Stage V–VI *Xenopus laevis* oocytes were prepared and injected with cRNA as previously described (Priel et al., 2006) prepared from pGEMHE plasmids carrying GluA1 (Q/flip), GluA2 (R/flip), HA-tagged SynDIG4 and EGFP-tagged TARPγ8. For giant outside-out patch recordings the vitelline membrane was removed using forceps. Recordings were performed at 17^{o}C, at membrane potential of -120 mV, using Axopatch 200B amplifier connected to digidata1322A and pCLAMP10.2 (Axon Instruments, Foster City, CA) and analyzed using ClampFit10.2 and Origin 8 (Origin Lab, Northampton, MA) software. For rapid solution exchanges, a double-barrel glass (theta tube) mounted on a piezoelectric translator (Burleigh, Fishers, NY) was used as

previously described (Priel et al., 2005). Patch electrodes were fabricated from borosilicate glass with a low resistance of 0.3-0.7 MΩ. AMPAR deactivation and desensitization were measured by applying glutamate (10 mM) for 1 ms and 500 ms, respectively. Recovery from desensitization was estimated with the two-pulse protocol in which a constant 100 ms application of glutamate (10 mM) was followed by a 100 ms test pulse applied at different time intervals. AMPAR-current deactivation and desensitization were fitted with two exponentials and the weighted tau (τ_w) was calculated as $\tau_w = (\tau f \times af) + (\tau s \times as)$, where af and as are the relative amplitudes of the fast (τf) and slow (τs) exponential component. *Statistical analysis.* Significance was compared with AMPAR expressed alone (*) or with AMPAR+TARPγ8 ($); *p*-value (one-way ANOVA): */$ < 0.05; **/$$ < 0.01; ***/$$$ < 0.001; ns, not significant.

Preparation of hippocampal slices. Mice were decapitated and brains put into ice cold dissection buffer (composition in mM: 127 NaCl, 1.9 KCl, 26 $NaHCO_3$, 1.2 KH_2PO_4, 10 dextrose, 2 $MgSO^4$, and 1.1 $CaCl_2$, saturated with 5% CO_2 and 95% O_2, final pH 7.4). The cerebellum was removed and forebrain slices were cut with a vibratome (Leica VT 1000A) and subsequently maintained in artificial cerebrospinal fluid (ACSF, in mM: 127 NaCl, 26 $NaHCO_3$, 1.2 KH_2PO_4, 1.9 KCl, 2.2 $CaCl_2$, 1 $MgSO_4$ and 10 D-glucose oxygenated with 95% O_2 plus 5% CO_2, final pH 7.4) for 1 hour at 30 °C and then for up to 5 hours at room temperature.

Field EPSP recordings in hippocampal slices. Field EPSPs (fEPSPs) were recorded as previously described (Matt et al., 2011). 400 µm thick slices from 8-12 week old mice were transferred into a submerged type recording chamber constantly perfused with oxygenated ACSF supplemented with 5 µM Bicuculline (Tocris) at 30°C. fEPSPs were recorded in the Schaffer collateral pathway with stimulation and recording electrodes positioned within the stratum radiatum near the CA3 region and recording electrodes in the CA1 region. fEPSPs were recorded using ACSF-filled glass pipettes (2-3 MΩ), amplified with an Axopatch 2B amplifier (Molecular Devices, CA), digitized at 10 kHz with a Digidata 1320A (Molecular Devices) and

recorded with Clampex 9 (Molecular Devices). Stimuli (100 μs) were delivered through a concentric bipolar electrode (TM53CCINS, WPI). The same intensity was used during baseline recording (0.067 Hz) and induction of LTP by tetanic stimulation. Tetanus paradigm consisted of 100 stimuli given at 100 Hz (1 sec). Theta-burst consisted of 10 bursts consisting of 4 stimuli at 100 Hz with a burst frequency of 5 Hz. The baseline was determined by the average of fEPSP initial slopes from the 10-minute period immediately before the tetanus. The level of LTP was determined by the average of fEPSP initial slopes from the period between 30 and 50 minutes after the tetanus. The same slices used for LTP recordings were used to record input-output relation (IOR) for stimulus intensities of 0.1 – 0.6 mA and paired-pulse facilitation (PPF) for inter-stimulus intervals of 10 ms, 20 ms, 50 ms, 100 ms, 200 ms, and to 500 ms (same stimulation strength as LTP recordings). For each data point, four individual traces were averaged. Data were analyzed and processed using Clampfit 9 and Microsoft Excel. Statistics and visualization were performed with GraphPad Prism. Results between genotypes were statistically compared using one-way ANOVA and Bonferroni's Multiple Comparison Test to compare baseline levels vs post-tetanus for both genotypes as well as post-tetanus levels between genotypes.

Whole-cell patch-clamp recording. 350 μm thick forebrain slices from P12-15 mice, prepared as described for extracellular recordings, were transferred into a submerged recording chamber constantly perfused with oxygenated ACSF supplemented with 5 μM Bicuculline at room temperature. Hippocampal pyramidal neurons were visually identified using an Olympus BX50WI upright microscope and an Olympus LumPlanFL 40x water-immersion objective with IR-DIC contrast through a Hamamatsu C2400 CCD camera. Patch micropipettes (2.5 – 5 MΩ) were filled with intracellular solution (in mM: 125 $CsMeSO_3$, 2.5 CsCl, 7.7 TEA, 4 Mg-ATP, 0.3 Na_2-GTP, 20 HEPES, 8 NaCl, 0.2 EGTA; pH 7.2) containing 5 mM QX-314 (Sigma) to prevent action potential firing. All patch-clamp recordings were made in whole-cell configuration using Clampex 9 to control an Axopatch 200B patch-clamp amplifier (Molecular Devices) through a Digidata 1322A digitizer. Cell capacitance and series resistance were monitored but not

compensated throughout experiments. Stimulation electrode was positioned in the stratum radiatum. Stimulus intensity was set to evoke 50% EPSC amplitude at a holding potential of -70 mV. Test pulses were given every 15 sec. After 5 min of baseline (no more than 8 min after break-in) cells were depolarized to 0 mV. After waiting 150 sec for accommodation, 180 pulses were applied with 2 Hz (90 sec) before the holding potential was switched back to -70 mV and test pulses resumed after 15 sec for 30 min. Signals were sampled at 10 kHz using a 2 kHz low-pass filter. LTP was determined using Clampfit 10 as the average EPSC amplitude recorded 15 – 30 min after pairing normalized to the average baseline EPSC. Results between genotypes were statistically compared using one-way ANOVA and Bonferroni's Multiple Comparison Test to compare baseline vs LTP for both genotypes as well as LTP between genotypes. For mEPSC recordings the extracellular ACSF was supplemented with 50 mM sucrose, 1 µM TTX (Tocris), and 5 µM Bicuculline. Cells were held at -70 mV and miniature events were sampled for up to 30 min at 2 kHz and filtered with a 1 kHz low-pass filter. Events were identified using Clampfit's inbuilt template-based event detection function. All events from one individual cell were averaged. Per-cell averages were used for statistical comparison between genotypes using unpaired t-tests. Analysis was performed using Microsoft Excel and GraphPad Prism.
Statistical analysis. GraphPad Prism 4.0 was used for statistical analysis. All data are shown as mean ± SEM. Significance levels are indicated by asterisks: n.s. not significant, * $p \leq 0.5$, ** $p \leq 0.01$, *** $p \leq 0.001$. Unless stated otherwise data were compared using one-way ANOVA and Bonferroni's Multiple Comparison Test against selected columns.

Behavior studies

Founder mice generated on a C57BL/6N genetic background were backcrossed four times (N4) onto the C57BL/6J strain to remove the *rd8* mutation (Mattapallil et al., 2012). Heterozygous N4 mice devoid of the *rd8* mutation were then intercrossed to produce WT and mutant (*SynDIG4*$^{-/-}$)

mice for behavioral experiments. Both males and females (ages 3-5 months) were used for behavioral testing at age (WT: 5 males and 4 females; *SynDIG4*$^{-/-}$: 3 males and 8 females). As no sex differences were detected on the cognitive scores, results from males and females were combined within genotype, to reach N = 9 WT, N = 11 *SynDIG4*$^{-/-}$. Mice were bred and housed on the UC Davis main campus and then transferred to the Sacramento campus for behavioral testing after a one-week habituation period. Researchers at the Sacramento facility were blinded to the genotype of the mice until after all behavioral experiments had been performed.

Morris Water Maze. Hippocampal-dependent spatial navigation learning and memory was evaluated using a standard Morris water maze (Vorhees and Williams, 2006). The Morris water maze was a 120 cm circular pool, filled 45 cm deep with water (24^{o}C) made opaque with non-toxic white paint (Crayola). External cues to aid spatial navigation included a prominent sink, computer, water temperature regulator with hose, a large black X on the wall and a yellow paper lantern hung from the ceiling. Trials were video recorded and scored by automated software (Noldus Ethovision, Wageningen, Netherlands) for measures including latency to find the hidden platform, total distance traveled, and swim speed. Mice were trained in the hidden platform version of the Morris water maze consistent with methods standard in the literature (Vorhees and Williams, 2006; Yang et al., 2012). Briefly, each mouse was placed into the water maze, facing the wall, in one of four possible quadrant locations, which differed pseudo-randomly by training day. Mice were given 60 seconds to find the hidden platform. If a subject mouse was unable to find the platform by the end of 60 seconds, it was gently guided to the platform and allowed to rest for ~10 seconds between trials. The hidden platform was in the same location, in the same quadrant, on each training day. Acquisition training consisted of four trials per day for five days. Trials were given sequentially, with an approximately 10 second platform rest interval. Mice were placed under infrared heating lamps after the last trial each day to prevent hypothermia. Acquisition was assessed daily until the WT group reached a latency criterion of <15 seconds to reach the hidden platform. Approximately 3 hours after the last training trial, the

platform was removed and mice underwent a 60 second probe trial to determine the amount of time spent exploring the target quadrant and the number of times the animal crossed the previous platform location and corresponding pseudo-platform locations in each quadrant.

Novel object recognition. The novel object recognition test was conducted in opaque matte white (P95 White, Tap Plastics, Sacramento, CA) open field arenas (40 cm x 60 cm x 23 cm), using methods similar to those previously described (Silverman et al., 2013a; Silverman et al., 2013b; Yang et al., 2012). The experiment consisted of three sessions, a 30 min exposure to the open field arena, a 10 min familiarization session and a 5 min recognition test. On day 1, each subject was habituated to a clean empty open field arena for 30 min. Twenty four hours later each subject was returned to the open field arena for the habituation phase, for 10 min. The mouse was then removed from the open field and placed in a clean temporary holding cage for approximately 2 min. Two identical objects were placed in the arena. Each subject was returned to the open field in which it had been habituated, and allowed to freely explore for 10 min. After the familiarization session, subjects were returned to their holding cages, which were transferred from the testing room to a nearby holding area. The open field was cleaned with 70% ethanol and let dry. One clean familiar object and one clean novel object were placed in the arena, where the two identical objects had been located during in the familiarization phase. Sixty minutes after the end of the familiarization session, each subject was returned to its open field for a 5 min recognition test, during which time it was allowed to freely explore the familiar object and the novel object. The familiarization session and the recognition test were videotaped and scored with Ethovision XT video tracking software (Version 9.0, Noldus Information Technologies, Leesburg, VA). Object investigation was defined as time spent sniffing the object when the nose was oriented toward the object and the nose-object distance was 2 cm or less. Recognition memory was defined as spending significantly more time sniffing the novel object than the familiar object. Total time spent sniffing both objects was used as a measure of general exploration. Time spent sniffing two identical objects during the familiarization phase confirmed

the lack of an innate side bias. Objects utilized were plastic toys; a small soft plastic orange safety cone and a hard plastic conical magnetic with ribbed sides.

Open field activity: Exploratory locomotion was assessed in individual mice using an automated VersaMax Animal Activity Monitoring System (AccuScan Instruments, Columbus, OH) for a 30 minute test session under low light conditions (40 lux), as previously described (Brielmaier et al., 2012; Flannery et al., 2015; Kazdoba et al., 2016; Silverman et al., 2011).

Elevated plus-maze anxiety-related behavior: Subject mice were placed in the center area of a black Plexiglas automated elevated plus-maze (Med-Associates, St. Albans City, VT), under 300 lux white light illumination, for a 5 minute test session, as previously described (Brielmaier et al., 2012; Flannery et al., 2015; Kazdoba et al., 2016).

Light↔dark anxiety-related behavior: Subject mice were placed in the light side of a two-chambered light↔dark apparatus for a 10 minute session, as previously described (Flannery et al., 2015; Silverman et al., 2011). Time in the dark chamber and number of transitions between chambers were automatically recorded using Labview 8.5.1 (National Instruments, Austin, TX).

Statistical Analysis. Data were analyzed using Graphpad Prism version 5.0 (Graphpad, La Jolla, CA). For the Morris water maze, latency was analyzed using Two-Way Repeated Measures ANOVA with Bonferroni's post-hoc tests. Probe trial data were analyzed using One-Way ANOVA with Bonferroni post-tests. Novel object data were analyzed using paired Student's t-test. Open field activity data were analyzed by the Mann-Whitney test. Elevated plus-maze and light↔dark activity data were analyzed with unpaired t-tests with Welch's correction. Data are presented as mean ± SEM.

Supplemental References

Brielmaier, J., Matteson, P.G., Silverman, J.L., Senerth, J.M., Kelly, S., Genestine, M., Millonig, J.H., DiCicco-Bloom, E., and Crawley, J.N. (2012). Autism-relevant social abnormalities and cognitive deficits in engrailed-2 knockout mice. PLoS One *7*, e40914.

Flannery, B.M., Silverman, J.L., Bruun, D.A., Puhger, K.R., McCoy, M.R., Hammock, B.D., Crawley, J.N., and Lein, P.J. (2015). Behavioral assessment of NIH Swiss mice acutely intoxicated with tetramethylenedisulfotetramine. Neurotoxicol Teratol *47*, 36-45.

Kazdoba, T.M., Hagerman, R.J., Zolkowska, D., Rogawski, M.A., and Crawley, J.N. (2016). Evaluation of the neuroactive steroid ganaxolone on social and repetitive behaviors in the BTBR mouse model of autism. Psychopharmacology (Berl) *233*, 309-323.

Matt, L., Michalakis, S., Hofmann, F., Hammelmann, V., Ludwig, A., Biel, M., and Kleppisch, T. (2011). HCN2 channels in local inhibitory interneurons constrain LTP in the hippocampal direct perforant path. Cell Mol Life Sci *68*, 125-137.

Mattapallil, M.J., Wawrousek, E.F., Chan, C.C., Zhao, H., Roychoudhury, J., Ferguson, T.A., and Caspi, R.R. (2012). The Rd8 mutation of the Crb1 gene is present in vendor lines of C57BL/6N mice and embryonic stem cells, and confounds ocular induced mutant phenotypes. Invest Ophthalmol Vis Sci *53*, 2921-2927.

Priel, A., Kolleker, A., Ayalon, G., Gillor, M., Osten, P., and Stern-Bach, Y. (2005). Stargazin reduces desensitization and slows deactivation of the AMPA-type glutamate receptors. J Neurosci *25*, 2682-2686.

Priel, A., Selak, S., Lerma, J., and Stern-Bach, Y. (2006). Block of kainate receptor desensitization uncovers a key trafficking checkpoint. Neuron *52*, 1037-1046.

Silverman, J.L., Babineau, B.A., Oliver, C.F., Karras, M.N., and Crawley, J.N. (2013a). Influence of stimulant-induced hyperactivity on social approach in the BTBR mouse model of autism. Neuropharmacology *68*, 210-222.

Silverman, J.L., Oliver, C.F., Karras, M.N., Gastrell, P.T., and Crawley, J.N. (2013b). AMPAKINE enhancement of social interaction in the BTBR mouse model of autism. Neuropharmacology *64*, 268-282.

Silverman, J.L., Turner, S.M., Barkan, C.L., Tolu, S.S., Saxena, R., Hung, A.Y., Sheng, M., and Crawley, J.N. (2011). Sociability and motor functions in Shank1 mutant mice. Brain Res *1380*, 120-137.

Vorhees, C.V., and Williams, M.T. (2006). Morris water maze: procedures for assessing spatial and related forms of learning and memory. Nat Protoc *1*, 848-858.

Yang, M., Bozdagi, O., Scattoni, M.L., Wohr, M., Roullet, F.I., Katz, A.M., Abrams, D.N., Kalikhman, D., Simon, H., Woldeyohannes, L.*, et al.* (2012). Reduced excitatory neurotransmission and mild autism-relevant phenotypes in adolescent Shank3 null mutant mice. J Neurosci *32*, 6525-6541.